Technical note: Determining Arctic Ocean [I.P]~~cold~~ halocline and cold halostad [I.P]~~layer~~ depths based on vertical stability

Enrico P. Metzner[1] and Marc Salzmann[1]

[1]Institute for Meteorology, Universität Leipzig, Leipzig, Germany,

Correspondence: Enrico P. Metzner (enrico.metzner@uni-leipzig.de)

Abstract. The Arctic Ocean [I.P]~~cold~~ halocline [I.P]~~layer (CHL)~~ separates the cold surface mixed layer (SML) from the underlying warm Atlantic W~~w~~ater (AW), and thus provides a precondition for sea ice formation. Here, we introduce a new method in which the [I.P]halocline~~CHL~~ base depth is diagnosed from vertical stability and compare it to two existing methods. [M.A.]Our main motivation for diagnosing the halocline base depth based on vertical stability was that v~~V~~ertical stability [M.A.]is closely
5   related to~~directly affects~~ vertical mixing and heat exchange[M.A.], and thus also to the role of the halocline in preventing vertical heat exchange and thereby protecting sea ice from warm AW. The second goal was to provide a particularly robust method. When applied to measurements from ice-tethered profilers, ships, and moorings, the new method for estimating the [I.P]halocline ~~CHL~~ base depth provides robust results with few artifacts. Comparatively large differences between [I.P]the~~our new method and two existing~~ methods for detecting the [I.P]halocline~~CHL~~ base depth were found in [I.P]warm AW inflow regions [I.P]for which
10   climate models predict increased net surface energy fluxes from the ocean to the atmosphere, suggesting that these regions may be particularly sensitive to a halocline retreat ~~most prone to a CHL retreat in a warming climate~~. [I.P]Analyzing a case in which water previously homogenized by winter convection was capped by fresh water at the surface suggests that the new method captured the beginning of new halocline formation in the Eurasian Basin. [M.A and I.P]~~CHL base depth exhibits a seasonal cycle with a maximum depth in winter and also spring, when the SML depth is also at its maximum, but the amplitude of the CHL~~
15   ~~base depth's seasonal cycle is lower than for the SML for all three methods as expected.~~ We also propose a novel method for detecting the cold halostad [I.P](CHS), which is formed by Pacific Winter Water (PWW) in the Canada Basin or by melt water [M.A and I.P]~~layer and study the seasonal cycle employing conservative assumptions to avoid a misclassification (including a lower bound of 50 m for the thickness). Detection of a cold halostad layer was largely confined to the Canada Basin and to the regions~~ off the eastern coast of Greenland and also Svalbard.

1   Introduction

20   The Arctic Ocean outside the main Atlantic warm water inflow and the shallow marginal shelf seas is usually stratified into a~~the~~ cold and fresh surface mixed layer (SML), which is from $\sim$5 to >100 m thick, depending on region and season (Peralta-Ferriz and Woodgate, 2015), [I.P]a~~the cold~~ halocline [I.P](CHL) below the SML with a base depth $\sim$40 to >200 m (Fig. 4 of Polyakov et al., 2018), [M.A.]~~and~~ a layer of warm and saline Atlantic Water (AW) below the [I.P]halocline~~CHL~~ centered near 300 to 500 m [I.P]in
25   the Eurasian Basin and somewhat deeper in the Canada Basin (Aagaard et al., 1981; Macdonald et al., 2015)[M.A.], and deep

water below. Convection in the SML is driven by surface cooling and brine release during sea ice formation, with maximum SML depth in winter. River inflow and precipitation act as sources of fresh water. [M.A and I.P]Below the SML, salinity increases in the halocline. Within the halocline, one can distinguish between the cold halocline layer (CHL) in the Eurasian Basin, the Pacific Halocline Waters (PHW, modified Pacific Water which originally entered the western Arctic via the Bering Strait) in the Amerasian Basin, and the lower halocline waters (LHW, water of Atlantic origin which is less modified compared to CHL water) (e.g. Alkire et al., 2017; Polyakov et al., 2018; Anderson et al., 2013). In the CHL, the temperature remains close to the freezing point. Several processes have been suggested as contributors to LHW and CHL formation. Based on data from the *Oden* 1991 cruise, Rudels et al. (1996) found that new halocline formation was initiated by the advection of relatively fresh shelf waters near the surface above denser and more saline water below, when the advection of the fresh water limited winter convection. Support for the importance of such a capping process was provided by lkire et al. (2017) and Rudels et al. (2004). They argued that capping by fresh water due to sea ice melting in the inflow from the Fram Strait and the Barents Sea can transform AW into halocline water. Another process which has been widely discussed, and which is thought to be especially important for the PHW is the advection of dense and saline shelf waters (where salinity increases due to brine release during sea ice formation especially in winter) below the SML (Aagaard et al., 1981; Jones and Anderson, 1986; Rudels et al., 2004). While halocline formation via capping does not require dense shelf waters, capping can also occur after (i.e. in addition to) the advection of dense shelf water (Steele and Boyd, 1998; Rudels et al., 2004). [M.A and I.P (added after discussion)]Steele and Boyd (1998) argued that seasonal capping by melt water in summer may not be overly important for insulating the SML from relatively warm AW. [M.A and I.P]The PHW in the Canada Basin originates from Pacific Water inflow, which is modified on the Chukchi Sea Shelf, but the LHW is of Atlantic origin also in the Canada Basin (e.g. Anderson et al., 2013). [I.P]Because of seasonal modifications on the Chukchi Sea Shelf, the PHW in the Canada Basin can be further subdivided into Pacific Winter Water (PWW) and less saline and warmer Pacific Summer Water (PSW) (e.g. Timmermans et al., 2014). The PWW could be referred to as a type of cold halocline water (Zhong et al., 2019), although compared to the CHL in the Eurasian Basin, in the PWW, the salinity is lower and the salinity gradient is smaller. This is why Shimada et al. (2005) called the layer which is formed by PWW a cold halostad (CHS). Similarly, interaction between glacial melt water and Arctic water north east of Greenland forms an intermediate [M.A.]low salinity [I.P]layer [M.A.]~~semi-saline layer of water~~ [I.P]with small salinity gradient which is also called a cold halostad (Dmitrenko et al., 2017). Below, we argue that a lower salinity and a smaller salinity gradient in the CHS compared to the LHW below results in two distinct local stability maxima between the base of the LHW and the SML base: The upper stability maximum is associated with an increase of salinity in the upper PWW. The lower stability maximum is associated with another increase of salinity in the LHW. The lower one of these two stability maxima is absent in the presence of a CHL in the Eurasian Basin (except in regions off the eastern coast of Greenland and also Svalbard where melt water also forms a CHS).

[M.A.]Because~~The CHL is also a pycnocline as~~ density is more influenced by salinity than temperature if the temperature is low (Aagaard et al., 1981; Roquet et al., 2022)[M.A.] a configuration with warm AW underlying colder halocline water ist stable. The presence of a (cold) halocline thus~~. Therefore, the CHL~~ insulates the SML from direct contact with the warm AW~~Atlantic water~~ [M.A.]and protects sea ice from the warm AW (Aagaard et al., 1981; Lind et al., 2016; Polyakov et al., 2017, 2020). Conversely,

~~But~~ a retreat of the CHL in the Eurasian Basin leads to increased vertical mixing as observed and described by Steele and Boyd (1998); Björk et al. (2002); Polyakov et al. (2017). [M.A.]Retreating sea ice, increased surface heat flux and the~~This~~ retreat of the [M.A.]halocline have been called~~CHL has been interpreted as a key feature of the increasing~~ atlantification of the [M.A.]Eurasian Basin~~Arctic Ocean~~ (Polyakov et al., 2017). Future climate model projections for a high emission scenario also showed [I.P]very large temperature gradients directly below the~~increasing atlantification with warm Atlantic water reaching the~~ surface mixed layer more frequently, especially during the cold season. [M.A.]The associated heating of the SML~~This increasing atlantification~~ in combination with sea ice loss resulted in further increased annual mean upward net surface energy fluxes outside the Central Arctic along the main warm water inflow pathways (Metzner et al., 2020). [I.P]While the halocline generally protects sea ice, PSW can be warm enough to participate in sea ice melting (e.g. Timmermans et al., 2014).

[M.A.]~~The CHL is characterized by a strong salinity gradient while temperature stays near the freezing point of sea water. Only a small proportion of the CHL is formed due to convection of brine during sea ice formation (Rudels et al., 1996; Alkire et al., 2017). Most of it is mixed and transformed water advected into the Arctic Basin from the shelves (Aagaard et al., 1981; Steele et al., 1995; Mu et al., 2017). The properties of halocline water and the vertical hydrographic structures are mostly studied locally from separated observations near shelves (Lien and Trofimov, 2013; Janout et al., 2017; Baumann et al., 2018) or by models of varying complexity (Jensen et al., 2016; Metzner et al., 2020). A notable exception is the study by Polyakov et al. (2018), who derived a map of the Arctic CHL base depth based on observations.~~

Several methods have been proposed for identifying the [I.P]halocline~~CHL~~ based on observations. Steele et al. (1995) identified cold halocline water based on conditions for salinity (34 <S<34.5 in the practical salinity scale) and temperature (T<-0.5°C). Rudels et al. (1996) defined the boundaries of the CHL by using the 34.3 isohaline. Bourgain and Gascard (2011) used a density ratio threshold to define the base of the [I.P]halocline~~CHL~~. [M.A.]~~This density ratio method was adopted among others by Polyakov et al. (2017, 2018) and Metzner et al. (2020).~~ The density ratio is the ratio of temperature and salinity contributions to the vertical stability. A large density ratio implies that the vertical stratification is dominated by temperature and a small density ratio implies that stratification is dominated by salinity. The density ratio threshold suggested by Bourgain and Gascard (2011) assumes that oceanic layers above the [I.P]halocline~~CHL~~ base are almost entirely salt-stratified with temperature contributing less than 5% to the total stratification (Polyakov et al., 2018). [M.A.]This density ratio method was adopted among others by others by Polyakov et al. (2017, 2018) and Metzner et al. (2020). [I.P]~~Bertosio et al. (2020) and Bertosio et al. (2022) distinguished between an upper and a lower CHL.~~ Using tracer observations in the western Eurasian Basin, Bertosio et al. (2020) found the base of the [I.P]LHW~~lower CHL~~ to be located at a density of 1027.85 kg m^{-3}. Analyzing salinity and temperature observations from the Makarov Basin and along the East Siberian continental slope, Bertosio et al. (2022) again defined the base of the [M.A and I.P]halocline using a ~~upper and the lower CHL based on~~ density threshold~~s~~ and compared the results obtained with th~~is~~ese definition~~s~~ to those obtained with other definitions from the literature. A[I.P]~~nother~~ fairly simple and robust method for computing the CHL base depth was proposed by Metzner et al. (2020). In this method, the base of the CHL is determined by a temperature difference of 1 [I.P]°C~~K~~ between water potential temperature and its freezing temperature. This temperature difference method is very sensitive to warming from below, while the density-ratio method of Bourgain and Gascard (2011) is very sensitive to the salinity profile. One drawback of the temperature difference method is a potential dependence of the

optimal threshold value on region (Metzner et al., 2020). Polyakov et al. (2018) proposed an indicator of the potential of the Arctic [I.P]halocline~~CHL~~ to prevent vertical mixing based on available potential energy, adapting the density ratio threshold of Bourgain and Gascard (2011) to identify the [I.P]halocline~~CHL~~ base.

[M.A]Here, we propose a new method to identify the halocline base using a vertical stability threshold and compare it to two existing methods using measurements from ice-tethered profilers, ships, and moorings. Our main objective was to devise a method that uses a threshold value of a variable which is closely related to the role the halocline plays for insulating the SML from the warm AW. The choice of a vertical stability threshold was~~Here, we define the CHL base based on vertical stability,~~ motivated by the argument that vertical stability is more directly related to vertical mixing than either density, temperature, or the density ratio. [M.A]Our second goal was to devise a particularly robust method to detect the halocline base. Based on the argument that the presence of PWW forming a CHS on top of LHW creates a stability profile with two distinct local stability maxima, we also propose a method for estimating the boundaries and the center of the CHS.[M.A]~~In the western Arctic, the CHL splits into an upper CHL and a lower CHL. In between lies water of Pacific origin entering the Arctic Ocean via the Bering Strait. This Pacific water is characterized by lower salinity than Atlantic water, but significantly higher salinity than fresh Arctic surface water (Lin et al., 2021). This leads to an intermediate layer called cold halostad layer (Shimada et al., 2005). Similarly, interaction between glacial melt water and Arctic water north east of Greenland forms an intermediate layer of semi-saline water with low salinity gradient which is also called a cold halostad (Dmitrenko et al., 2017).~~ Consistent and robust descriptions of the [I.P]halocline~~CHL~~ and cold halostad layer boundaries are important to understand the evolution of the structure of the upper Arctic O~~o~~cean in the past and the future.

[M.A]In the next section, we first describe methods to determine the halocline base depth, starting with two existing methods which are used for comparison, i.e. the density ratio (DR) method by Bourgain and Gascard (2011), and the temperature difference (TD) method by Metzner et al. (2020). We then introduce our new stability (ST) method for determining the halocline base depth. In Section 2.2, we propose a new method for estimating the CHS upper and lower boundaries and the CHS center, which is based on vertical stability as well. In Section 2.4, we describe a method for estimating the SML base depth because the downward search for the DR and the TD threshold starts at the SML base and because the top of the halocline is assumed to coincide with the SML base. In Sect. 2.5, we introduce observational datasets used for comparison and testing. In Sect. 3, we compare the new ST method for determing the halocline base depth to the existing methods and test the new method for determining the CHS depth and extent. We first compare the methods to determine the halocline base using case studies and investigate whether the ST method captures the beginning of new halocline formation based on a suggestion in a reviewer comment on the original submission by Polyakov in Sect. 3.1. We then use maps and basin-wise statistics (based on a suggestion in a reviewer commment by Athanase, 2023) in Sect. 3.2. The performance of the CHS algorithm is discussed in Sect. 3.5. The results are summarized and discussed Sect. 4. ~~Here, we propose new diagnostics for the CHL base and the cold halostad layer boundaries and compare our results for the CHL base to the result from two previously suggested methods. The observational datasets on which our analysis is based are introduced in Sect. 2.5. Details of the density ratio (DR) method by Bourgain and Gascard (2011), the temperature difference (TD) method by Metzner et al. (2020), and the new stability (ST) method are provided in Sect. ??. The top of the CHL is assumed to coincide with the base of the SML (see Sect. ??). We use the~~

kriging method to produce continuous maps of CHL and cold halostad layer boundaries (as explained in Sect. ??). Results are discussed in Sect. 3.

Please note: We re-arranged the following section to introduce methods before introducing data.

2 Methods and DataMaterials and Methods

135 **2.2 Determining the vertical structure**

2.1 Methods for estimating the halocline base depth

2.1.1 DBase depth estimate by the density ratio (DR) method

[M.A and I.P]In a halocline, the density gradient due to temperature must be small compared to the density gradient due to salinity by definition (Bourgain and Gascard, 2011). The density ratio (DR) method by Bourgain and Gascard (2011) therefore identifies

140 the halocline base by the requirement that the ratio R_ρ between the density gradient due to temperature and the density gradient due to salinity must remain below a certain threshold. The density ratio is defined as The base of the CHL was estimated with three different methods. The first method (Bourgain and Gascard, 2011) uses the density ratio $R_\rho = \left(\alpha \nabla_z \theta_{\mathrm{pot}} \right) / (\beta \nabla_z S)$ **Please note: The track changes package we use does not handle subscripts correctly. The subscript "pot" was removed and not added.** with potential temperature θ_{pot} in °CKPlease note: This does not make difference for the gradient, salinity

145 S in the practical salinity scale and depth z in m. $\alpha = \underline{-}\rho^{-1}(\partial\rho/\partial\theta_{\mathrm{pot}})$**Please note: Sign of α corrected** and $\beta = \rho^{-1}(\partial\rho/\partial S)$ are the thermal expansion coefficient and the haline contraction coefficient, respectively. Bourgain and Gascard (2011) empirically estimated that searching downward for the depth, in which R_ρ exceeds 0.05, provides a reasonable estimate for the base of the [I.P]haloclineCHL. The search starts at the base of the SML (here determined as described in Sect. 2.4 below), which is defined to be the top of the halocline layerThe density ratio represents the slope in the temperature(θ)-salinity(S) diagram

150 scaled by α and β and is a proxy for the transition between a halocline and a thermocline. This method will subsequently be referred to as the density ratio (DR) method. [M.A.]If the density ratio threshold is exceeded already directly at the base of the SML, then no halocline was detected for the corresponding profile. Such profiles are excluded when computing statistics of halocline base depths. Similarly to Bourgain and Gascard (2011), we smoothed the S and θ prior to computing the density ratio as explained in Sect. 2.5.

155 #### 2.1.2 [I.P]TCHL base depth estimate by the temperature difference (TD) method

The temperature difference (TD)second method (Metzner et al., 2020) uses the difference ΔT between the ocean temperature $T\theta$ and the sea water freezing temperature T_{freeze} [M.A.]to estimate the cold halocline base depth. The freezing temperature was calculated from Gill (1982). [M.A and I.P]Searching downward, starting at the SML base, tThe base of the [I.P]haloclineCHL was calculated as the depth, in which ΔT first exceeds $1\,\mathrm{K}$. This threshold was estimated to be high enough, that the "cold"

160 core of the [I.P]cold halocline layerCHL is detectable, and low enough to separate the CHL from the AWAtlantic water with

core temperature approximately $1.5\,°C$ to $3\,°C$ ($T_{\text{freeze}} \approx -2\,°C$ leads to $\Delta T \approx 3.5\,°C$ to $5\,°C$ at the core). In cases in which the temperature threshold was first exceeded in a depth [I.P]shallower~~smaller~~ than $80\,\text{m}$, the search was continued $0.5\,\text{m}$ below this depth. [I.P]If the temperature threshold was exceeded already at the SML base, no halocline was detected. The algorithm was applied to smoothed temperature data (see Sect. 2.5).~~This method will be referred to as the temperature difference (TD) method.~~

2.1.3 [I.P]CHL base depth estimate by the s~~S~~tability (ST) method

The new stability (ST)~~third~~ method prescribes a threshold for~~uses~~ the local vertical stability in order to estimate the halocline base depth. Vertical stability is more closely related to vertical mixing than either the density ratio or the temperature difference. Because the search direction was found to affect the robustness of the method, and because stability is decreasing with depth between the AW and the core of the halocline, we search upward instead of downward for the stability threshold~~as parameter, which is directly linked to vertical mixing~~. The stability was computed from $L = \log_{10}(N^2)$, where $N = \sqrt{-(g/\rho)\,(\partial\rho/\partial z)}$ is the Brunt-Väisälä-frequency (with density computed from pressure, smoothed S, and θ as described below). The stability threshold was approximated~~is~~ based on the density ratio threshold $R_\rho = 0.05$ assuming an approximately constant salinity gradient near the halocline base in the LHW. It was derived starting from the following relationship:

$$\rho^{-1}\nabla_z\rho \;=\; \beta\nabla_z S \;-\; \alpha\nabla_z\theta_{\underline{\text{pot}}} \;=\; \beta\nabla_z S(1 - R_\rho) \tag{1}$$

With stable $\beta = (7.82 \pm 0.03)\cdot 10^{-4}$ over a wide range of temperature, salinity and pressure values ($-1.2\ldots2.0\,°C$, $32\ldots37$, $50\ldots350\,\text{dbar}$) and the salinity gradient in m^{-1}:

$$L \;=\; \log_{10}(-\nabla_z S) - 2.137 \pm 0.002 \tag{2}$$

Expecting the salinity gradient to be around $0.01\,\text{m}^{-1}$ near the base of the halocline, the resulting stability threshold should be $L \approx -4.14$.

This threshold is searched from $600\,\text{m}$ or at the lowest point (at least $500\,\text{m}$ deep outside the shallower regions according to the conditions for including profiles in the analyses described below in Sect. 2.5~~above~~) to the surface, as no CHL base was observed deeper than that~~ and stability is mostly decreasing with depth below the CHL and SML~~. Seldom, the first estimate is in warm [I.P]AW at $T > 0°C$~~water (detected by $\Delta T > 2\,\text{K}$, doubled DT-threshold for safety) due to measurement uncertainties in the temperature and salinity profiles~~. In such cases, a second search for the stability threshold is started slightly above. [M.A.]If the stability threshold is never exceeded or only exceeded where $T > 0°C$ in a given profile, then no halocline base was detected for this profile. ~~When the maximum stability is lower than the threshold, which can happen in shallow regions, the temperature difference ΔT at the base of the SML was checked against the threshold from the TD method. If ΔT is greater than $2\,\text{K}$, the water mass was considered Atlantic water and the CHL thickness was set to zero. Otherwise, the algorithm failed and a fill value was returned. This method will be further referred to as stability (ST) method.~~ **Please note: We simplified the explanation. Whether the halocline thickness was set to zero or treated as a missing value does not make a difference because in the end, both are treated as "no halocline detected".**

2.2 Cold hHalostad (CHS) boundary and center estimates

[I.P]A CHS is formed by PWW in the Canada Basin and also by melt water off the eastern coast of Greenland and Svalbard.
195 Compared to the CHL in the Eurasian Basin, a CHS is characterized by a smaller salinity gradient because of the different water origins. As demonstrated below, this leads to one local stability maximum at the top of the CHS (at the transition between SML or PSW and PWW) and a second stability maximum associated with the transition between CHS and the LHW. The stability minimum between these two local stability maxima is associated to the CHS. Therefore, as a first condition for identifying a CHS, we require that more than one local stability maximum must be present between the base of the SML and
200 the base of the halcoline as identified by the ST algorithm described above. **Please note: We failed to mention the following point in our original manuscript. The operation described below is applied in addition to the requirement that the vertical extent of the local minimum must be at least 50 m** [M.A.]Because the stability profiles computed from temperature and salinity observations contain small scale fluctuations even after smoothing the S and θ data that is used for computing density as described below, we identify local maxima by first computing a "moving" stability maximum for a 50 m vertical box
205 surrounding each observation. This moving stability maximum is computed from $L_m(z) = \max\left(L(z') \text{ for } |z' - z| < 25\,\text{m}\right)$, where z is depth. This moving maximum operation was defined in analogy to a moving average. The result is a profile of stability maxima $L_m(z)$ with few local maxima. [I.P]We then compute the mean of the lower stability maximum, which is associated with the transition between CHS and LHW, and the stability minimum between the upper and the lower stability maximum, which is associated with the CHS.~~In case of multiple stability maxima in the vertical profile, the thickness and~~
210 ~~the depth of the cold halostad are estimated. The cold halostad separates the CHL into an upper and a lower branch. It is associated with a stability minimum between two stability maxima. In order to estimate the thickness of the cold halostad, we first compute the mean of the stability minimum and the stability maximum associated with the lower branch of the CHL.~~ This value is used [I.P]as a threshold to define the [I.P]upper and the lower boundary of the CHS~~the boundaries of the cold halostad~~. The depth of the [I.P]center of the CHS~~cold halostad~~ is [I.P]define~~destimated~~ as the mean of the upper and lower bound[I.P]ary of the
215 CHS. A CHS~~cold halostad~~ will only be recognized by the algorithm if the vertical distance between [M.A.]the deeper stability maximum the first upper occurrence of that same stability value is at least 50 m, and [M.A.]the difference of L between the lower stability maximum and the local minimum in the CHS is at least 0.2~~this stability layer has at least a relative depth of 0.2 in~~ ~~$\log_{10}(N^2)$~~. [M.A.]With this definition, we never identified more than a single CHS per profile.~~In rare cases, in which more than one layer fulfills these conditions, only the lowest of these layers is identified as a cold halostad.~~

220 ## 2.3 [I.P]~~Occurrence frequency of the CHL and cold halostad~~

Please note: We now explain more explicitly what it means that no halocline was detected for a given profile above, omitting technical details, especially the treatment of rounding errors in floating point operations. Based on this, the occurrence frequency is now defined below in the results section. [I.P]~~Occurrence frequencies of the CHL were computed for each method individually based on whether the criteria for estimating the CHL base depth were satisfied. Furthermore, a~~
225 ~~lower threshold of 0.001 m was used for the CHL thickness, below which no distinctive layer is assumed to exist. Cases in~~

which either the criteria was not satisfied or else the thickness was computed to be less than $0.001\,\mathrm{m}$ were the classified as "no CHL". This includes cases in which the CHL and the SML bottom coincide within numerical accuracy and cases in which we initially computed a value for the CHL base depth that was smaller than the value for SML base depth.

[I.P]The depth of the cold halostad layer was computed whenever data was available and the conditions for identifying a cold halostad layer as described above were fulfilled. The occurrence frequency for the cold halostad layer was only computed for a region in the Canada Basin. Outside this Canada Basin region, the occurrence frequency was not computed due to the sparsity of observations in these regions.

2.4 SML depth estimate

The SML depth was estimated by a change in potential density of $0.125\,\mathrm{kg\,m^{-3}}$ at the surface as in Polyakov et al. (2017). In cases, in which a CHL is detected, the depth of the SML corresponds to the top of the CHL. Potential density was computed from smoothed S and θ.

[M.A and I.P]### 2.3 Kriging

[M.A and I.P]The estimates of the SML thickness, the CHL base depth and the occurrence frequency of the CHL are inter- and extrapolated with kriging. Kriging (e.g. Deutsch, 1994) is a tool from geostatistics for interpolation, extrapolation and smoothing at locations without direct measurements by data from surrounding observations. Those observations are weighted together depending on the local variability estimated by a multidimensional autocovariance function. The latter is approximated with a so called semi-variogram model. In this analysis only the spherical semi-variogram model is used (Mert and Dag, 2017; Reshid, 2019). The weights take into account the clustering of the observations as it uses the inverse of the correlation-distance matrix between input points and the correlation-distance vector between input points and the point of interest. All inter-/extrapolation weights are calculated from the location and distribution of given information without prior knowledge of ocean currents.

[M.A and I.P]Here, kriging was performed on an azimuthal-equidistant projection. The North Pole was used as the central reference point. $0°\,E$, $90°\,E$, $180°\,E$ and $90°\,W$ are on negative y-axis, positive x-axis, positive y-axis and negative x-axis respectively. The resolution is $0.46875°$ or roughly $52\,\mathrm{km}$ at the North Pole. The year was equally separated into 12 periods to simplify calculations and time averaging afterwards. This lead to $36 \times 12 = 432$ time steps and a temporal resolution of about $30.4\,\mathrm{days}$.

[M.A and I.P]Each quantity was prepared for kriging in three steps:

1. [M.A and I.P]A spatial trend of the time mean was computed.

2. [M.A and I.P]Outliers were removed for each season separately. Data values were identified as outliers if the difference to the spatial trend was lower (higher) than the $25^{th}(75^{th})$ percentile decreased (increased) by 1.5 times the inter quartile range.

3. [M.A and I.P]The spatial trend was subtracted from the raw data. The resulting anomalies were normalized to ensure a nearly constant variance for the entire Arctic.
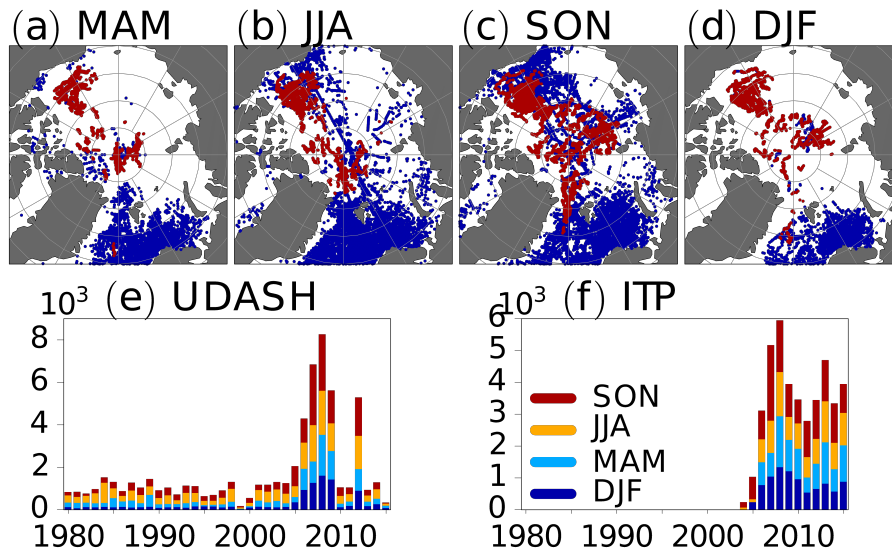
Figure 1. **Please note: Revised figure. The figure differs from the corresponding figure in our response to the reviewer comment by I. P. because we omitted low resolution profiles form the UDASH data set as described in the revised manuscript.** ^{I.P.}L~~Map of data locations~~ of observations for each season ^{I.P.}(starting with MAM for March, April, and May) with blue dots for UDASH profiles and red dots for ITP profiles **(a–d)**. Temporal coverage for UDASH **(e)** and ITP **(f)** observations. ~~Background is separated into similar regions as in the UDASH dataset (Behrendt et al. (2018): Amerasian Basin (light blue), Eurasian Basin (light red), Barents Sea (light green), Shelf regions (light yellow), North Atlantic (orange) and Canadian Shelf (white).~~

^{M.A and I.P}~~After kriging, the results were rescaled back to local variance and the spatial trend was added to retrieve the original local value range. Removing outliers and subtracting spatial trends are common practice in kriging. The code, which was used in this study, is available on GitHub with version v0.0.5 from http://doi.org/10.5281/zenodo.7572759.~~

2.5 Data and preprocessing

T~~In this study, t~~emperature and salinity observations were taken from the ice tethered profiler (ITP) project (Krishfield et al., 2008; Toole et al., 2011) and the Unified Database for Arctic and Subarctic Hydrography (UDASH, Behrendt et al., 2018). The ITPs measured temperature, salinity, and pressure twice a day while drifting with the ice floe they were tethered to. ^{Moved down, Rev. #2}~~ITPs deployed in the Arctic Ocean before 2018 were included here.~~^{M.A.}Data processing for the ITP data is described by Krishfield et al. (http://www.whoi.edu/fileserver.do?id=35803&pt=2&p=41486). Here, we used processed ITP Level III data. Producing Level III data included removal of corrupted data, corrections for the sensor response behavior, calibrations, and final screening of spurious outliers. ^{Moved here, Rev. #2}ITPs deployed in the Arctic Ocean before 2018 were included here. ^{I.P}The vertical resolution for ITP level III data is 1 ± 0.1 dbar. The accuracy of the sensors used for the ITP observations is $0.002°C$ for temperature and 0.002 for salinity (Polyakov et al., 2017). ^{I.P}~~Level III data was binned to two-day intervals in order to reduce noise and to reduce the number of missing columns in favor of a continuous time series.~~ ^{Moved here, Rev. #2}The

UDASH data set contains data from ships, ice-tethered profilers, profiling floats and other platforms (Behrendt et al., 2018). ~~OFrom the UDASH data set, o~~nly profiles, for which both temperature and salinity were available, were analyzed here. [I.P.]Furthermore, only profiles with a vertical resolution finer than 2.5 dbar in the upper 300 m and a vertical resolution finer than 5 dbar elsewhere were used~~Of this subset of profiles, all profiles were used, which start closer to the surface than 5 m~~

275   ~~in order to obtain a stable estimate for the SML.~~[Moved up, Rev. #2]~~The UDASH data set contains data from ships, ice-tethered profilers, profiling floats and other platforms (Behrendt et al., 2018).~~ We also required that the deepest point in a profile must reach at least 500 m or 90% of the basin depth~~Our analysis was limited to profiles that reach at least a depth of 500 m except in shallower regions, where the condition was that the profiles must reach down to 90% of the ocean bottom depth~~. This choice addresses the issue of potential sampling biases due to limited vertical exten~~t~~d of the observed profiles. [I.P.]Regions shallower

280   than 100 m were always excluded from the analysis. Bathymetry data was taken from the General Bathymetric Chart of the Oceans (GEBCO) dataset (GEBCO Bathymetric Compilation Group 2021, 2021). [I.P.]This filtering left a total of 43715 ITP and 62012 UDASH profiles. Fig. 1 provides an overview of the spatio-temporal coverage of the data.~~This resulted in 116814 (pairs of) temperature and salinity profiles whose locations are shown in Fig. ??.~~ **Please note: This fairly small difference between the total number of profiles compared to the original manuscript stems from a compensation between additional fil-**

285   **tering (decreasing the number of profiles analyzed) and no longer binning the ITP data to two-day intervals as before (increasing the number of profiles analyzed).** Most measurements are concentrated in the Barents Sea and only few were taken in the Central Arctic during winter. For the East Siberian Sea and the interior of the Laptev Sea, no data was available for winter and spring. Salinity was given in the practical salinity scale.

     Depth was computed from pressure using the hydrostatic equation. Density was computed based on salinity, temperature,

290   and pressure.~~For profiles, for which only depth was reported, pressure computed iteratively based on temperature, salinity and depth as in Metzner et al. (2020). For profiles, for which only pressure was reported, depth was computed.~~**Please note: All observations used here were reported on pressure levels. Mentioning iterations was an error. An iterative approach was only applied to model data, which we did not use here.** [I.P.]~~All values were regridded to the same vertical high-resolution grid with 0.5 m resolution in the first 50 m of the upper ocean and 1 m resolution down to 200 m depth, and 2 m between 200 and~~

295   ~~400 m depth. Below this, the resolution decreased to 2.5 m at 772.5 m depth. This results in 500 vertical grid points.~~[M.A.]In order to reduce noise, S, T, and/or θ were smoothed using a standard one-dimensional Gaussian filter (convolution with a Gaussian function, e.g. Deng and Cahill, 1993) with a standard deviation of 2 dbar and a truncation at ± 10 dbar.~~After regridding, a Gaussian filter with a standard deviation of 5 m and a truncation at ± 15 m was applied.~~ When using thresholds to estimate the SML or CHL base depth, variables were linearly interpolated between two adjacent depths. Consequently, the SML or CHL

300   base can be located between two vertical [I.P.]observation~~grid~~ points and the SML and CHL base depths do not necessarily have to coincide with the depths of the [I.P.]observations~~grid points~~.
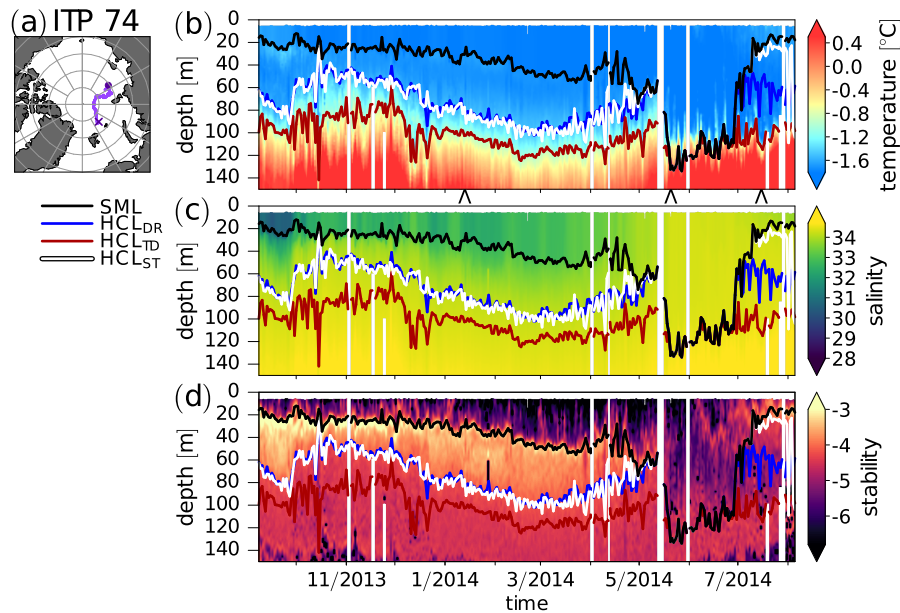
Figure 2. Please note: Revised figure using level III data without regridding. ITP-74 <s>L</s>location of measurements **(a)** and time series of <s>(a)</s> temperature **(b)**, <s>, (b)</s> salinity **(c)**, and <s>(c)</s> vertical stability **(d)**<s>along the path of ITP 74</s>. The circle and the cross in (a) mark the beginning and the end of the ITP-74 track, respectively. The colored lines in (b–d) are the base of the SML (black) and the ^{I,P}halocline (HCL)<s>CHL</s> base depths derived by the DR method (blue), the TD method (red) and the ST method (white). Salinity is given in the practical salinity scale. ^{M,A and I,P}Individual profiles at the location of the wedge symbols (∧) below the x-axis in (b) are shown in Fig. 3. Profiles that started below 15 m were excluded (only) in this figure (but nowhere else), because this increased readability by reducing the effect of noise in determining the SML base without affecting the overall result.

3 Results

3.1 ^{I,P}Comparison of methods for deriving halocline<s>CHL</s> base depth using case studies

<s>In</s> Figure 2<s>, we</s> compares three different methods for determining the ^{I,P}halocline<s>CHL</s> base depth for ITP-74. Starting from the Laptev Sea in September<s>October</s> 2013<s>2</s>, ITP-74 drifted across the Central Arctic, almost reaching the East Greenland Sea ^{M,A and I,P}(Fig. 2a). Until May 2014, ^{M,A and I,P}Fig. 2b–d shows<s>there is</s> evidence of a well-defined and stably stratified CHL ^{M,A and I,P}below the SML. The vertical stratification observed by ITP-74 prior to May 2014 and the performance of the three methods for determining the halocline base depth are further analyzed in an individual profile from this period in Fig. 3. Individual profiles of salinity and temperature for 13 January 2014 in Fig. 3a show the base of the SML at about ∼30 m. Between the SML base and ∼80 m a strong salinity gradient and temperatures close to the freezing point indicate a well defined CHL, which is ∼60 m thick. Between the CHL and the AW, temperature and salinity increase in the LHW. Below ∼170 m warm and saline AW is found (please note that at ∼170 m, the temperature and salinity slopes in Fig. 3a both change). Figs 3b–d show the density ratio, the temperature difference, and the stability for the observations on 13 January 2014 together
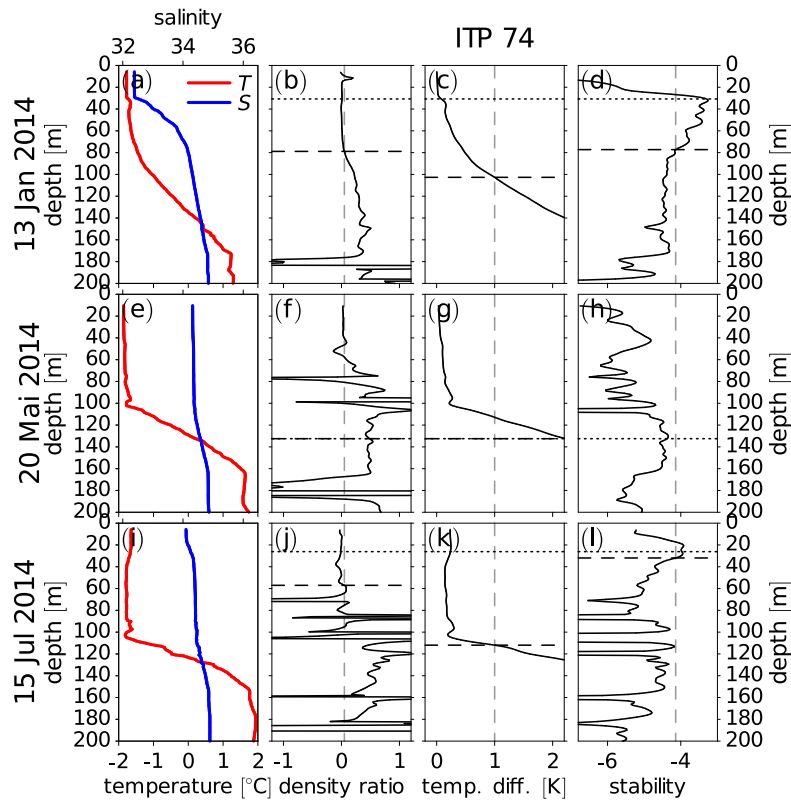
Figure 3. **Please note: Figure added based on suggestion by both reviewers. In our response to the reviewer comment by M. A. Figure 3h accidentally showed a dash-dotted instead of a dotted line. This was corrected.**[M.A and I.P]Temperature T and salinity S, density ratio, temperature difference, and stability from ITP-74 before winter convection on 13 January 2014 **(a–d)**, during winter convection on 20 May 2014 **(e–h)** and after winter convection on 15 July 2014 **(i–l)**. Vertical dashed lines indicated threshold values. Horizontal dashed lines indicate the halocline base determined by the three different methods. Dotted lines indicate the SML base. Dash-dotted lines in (f) and (g) indicate that a threshold for identifying the halocline base was exceeded at the SML base.

with the threshold values used to identify the halocline base with the DR, the TD, and the ST method. For the profile observed
315   on 13 January 2014, the DR method (Fig. 3b) and the ST method (Fig. 3d) identify the CHL base, while the TD method (Fig. 3c) places the halocline base in the LHW, somewhere between CHL and AW. The stability profile in Fig. 3d yields distinctly different stabilities for the SML, the CHL, the LHW, and the AW~~separating the less stably stratified Atlantic water from the SML~~.

      In May 2014, the SML deepens and the CHL disappears (Figure 2), as previously noted by Polyakov et al. (2017). [M.A and I.P]During
320   this convection event, neither of the three methods identified a halocline. Figs 3e–h show profiles for 20 May 2014 after the onset of convection. On this date, the threshold for identifying the halocline base was already exceeded at the SML base for the DR and the TD method (Fig. 3f and g), while the threshold was not reached for the ST method (Fig. 3h). After July, the situation becomes [I.P]particularly interesting~~less clear~~. The stability at about 80 m depth remains low, ~~possibly~~ pointing to~~at~~ the

residual of a mixed layer well below the diagnosed SML base [I,P](Figure 2). Fig. 3i for 15 July 2014 (after convection) also shows freshening and warming near the surface. This indicates that relatively fresh melt or/and shelf water may have been advected above a colder and saline layer, which had previously been homogenized by winter convection. The freshening near the surface leads to a salinity gradient below, and also a stability maximum, which is captured by the ST method (Fig. 3h). This appears to be consistent with the mechanism for halocline formation described by Rudels et al. (1996). As stated above, Rudels et al. (1996) found new halocline formation taking place when relatively fresh shelf waters near the surface were advected above denser and saltier water below, limiting winter convection, while Rudels et al. (2004) and lkire et al. (2017) stressed the role of melt water in general (including non-shelf water) in the warm Atlantic inflow through the Fram Strait and the Barents Sea for halocline formation via this type of capping mechanism. Fig. 2 suggests that in this particular case, the convection affected halocline water. This is also consistent with a study by Steele and Boyd (1998), who suggested that the capping mechanism can act in addition to the advection of dense and saline shelf waters. In the Steele and Boyd (1998) mechanism, which combines findings by Rudels et al. (1996) with earlier findings (e.g. Aagaard et al., 1981), high salinity in the capped water derives from advected cold and dense shelf water, which may previously have been affected by brine release in shelf seas, and not directly from AW. Here, the origin of the halocline water is unclear. However, Fig. 3h for 15 July 2014 (after winter convection) suggests that the ST method might indeed be useful for identifying the beginning of new halocline formation via the Rudels et al. (1996, 2004) capping mechanism or the Steele and Boyd (1998) mechanism which essentially assumes that the Rudels et al. (1996) capping mechanism acts in addition to the advection of dense shelf water (e.g. Aagaard et al., 1981). Below this layer, warm Atlantic water is found (Fig. ??b, compare also figure 3b of Polyakov et al., 2017). The origin of the fairly stable intermediate layer centered at about 20 m is less clear.

[I,P]The CHL base depth as diagnosed by the DR and the ST method agree well until May 2014. Both methods trace the pronounced stability gradient at the CHL base (Fig. ??d). The TD method, which is less sensitive to the salinity gradient by design, instead traces the temperature gradient in Fig. ??b and places the CHL base about 20 m below the base as identified by the DR and the ST method. Neither the ST nor the TD method show spurious depth minima reaching the SML for this particular ITP.

[I,P]During the final months, when the SML is diagnosed to be rather shallow, the DR method diagnoses a somewhat thicker CHL compared to the ST method. The TD method again traces the temperature gradient in Fig. ??b. The CHL base diagnosed with the DR method during the final months is ~20 m below that diagnosed by Polyakov et al. (2017) using the same method and the same input data, albeit without prior temporal averaging and vertical smoothing. Before the deepening of the SML in May 2014, the CHL base depth from the DR method agrees well with Polyakov et al. (2017), except noise. On the one hand, binning the data in to two-day intervals results in a smoother CHL base compared to figure 3 of Polyakov et al. (2017). On the other hand, spurious depth minima still occur. As in Polyakov et al. (2017) and Metzner et al. (2020), such spurious minima can reach all the way to the SML. Spurious minima are also found for other ITPs, but not for all ITPs. Furthermore, not only the DR method but also the TD method occasionally yields spurious minima (Supplement 1, see also discussion of Fig. RM3 below). However, for the model data analyzed in Metzner et al. (2020), warm Atlantic water was indeed often found directly
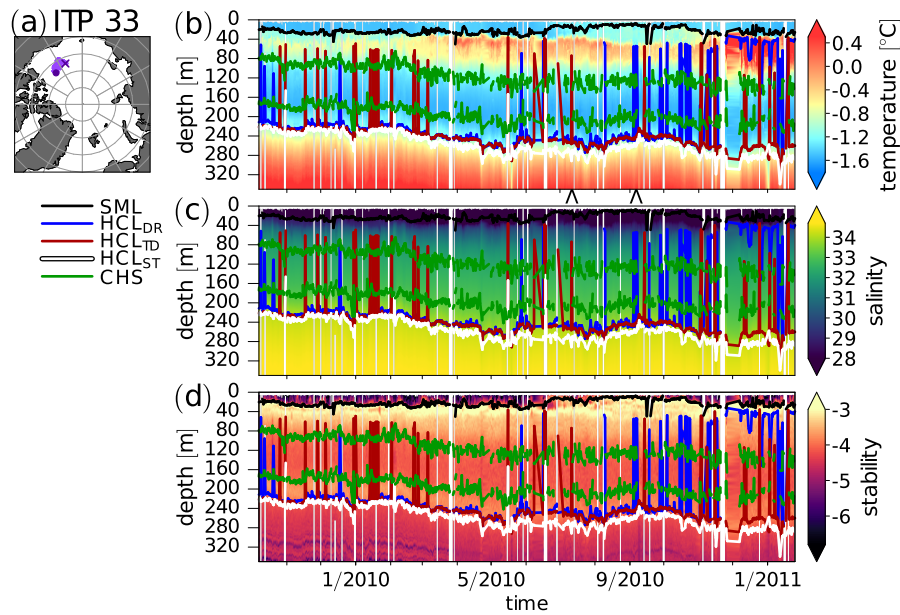
Figure 4. **Please note: Revised version of figure 8 moved to here** ~~A~~Same ~~as~~ as Fig. 2[M.A and I.P] buta ~~and d~~ for [M.A and I.P] ~~(top)~~ ITP-33[M.A and I.P] ~~and (base) ITP 29~~. Additionally, the results of the cold halostad bound estimation are shown in dark green.

~~underneath the SML during halocline thinning events. Artifacts such as the spurious CHL base depth minima found in Fig. **??** for the DR method are nevertheless a reason for concern.~~

360   [M.A and I.P]Figure 4 again compares the three different methods for determining the halocline base depth, but this time for ITP-33, which drifted in the Canada Basin between October 2009 and January 2011, where it encountered PSW on top of PWW. In addition to the halocline base depth, Fig. 4b–d shows the CHS boundaries which have been estimated based on stability as described above. The performance of the new algorithm for identifying the CHS will be discussed further below. For now, the main focus will be on isolated spurious minima of the halocline base depth. As evidenced by the spikes in Fig. 4b–d,

365 such isolated spurious base depth minima occur for the DR and the TD algorithm, but not the ST algorithm. Reasons for the occurrence of these artifacts will be further analyzed based on Figure 5. Figure 5a–d shows a case from ITP-33 on 11 July 2010 in which the TD method produced an isolated halocline base depth minimum and Fig. 5e–f shows a case on 6 September 2010 in which the DR method produced an isolated halocline base depth minimum. In both cases, the isolated minima are related to a layer of warm PSW around ∼80 m (Figs. 5a and e, compare also Fig. 4b). For 11 July 2010, the best estimate of the halocline

370 base depth is provided by the DR method (Fig. 5b). The DR method correctly places the base of the halocline water at a depth, where the salinity gradient (Fig. 5a) changes. Stability (Fig. 5d) also decreases markedly at this depth, although the ST method identifies the halocline base about 20 m below this location (Fig. 5d). The TD method (Fig. 5c) places the halocline base at about 80 m in the layer of warm PSW, although the salinity gradient below this layer still indicates the presence of a halocline and temperature decreases below this layer, indicating PWW. For 6 September 2010, the DR threshold is exceeded at a local
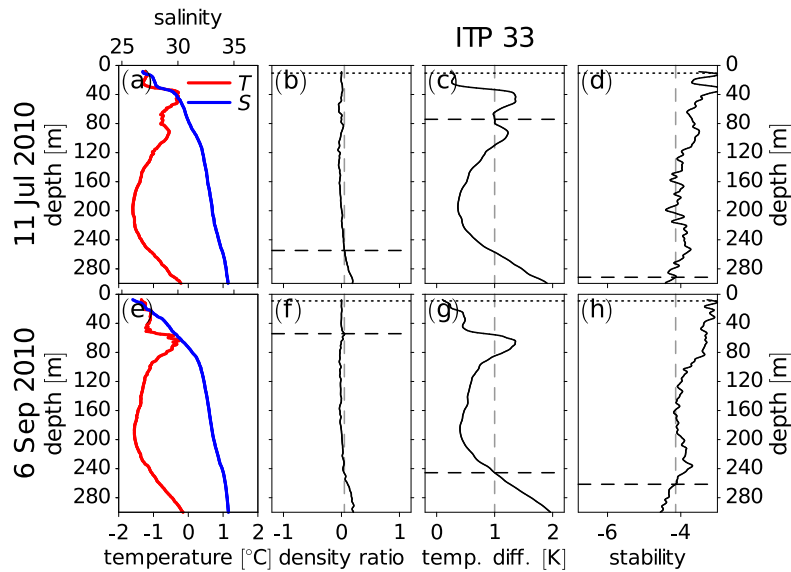
Figure 5. **Please note: Figure added based on suggestion by both reviewers** [M.A and I.P] As Figure 3, but for two profiles from ITP-33. For 12 July 2010 **(a–d)** the TD method shows an isolated minimum of the halocline base depth, and for 6 September 2010 **(e–f)** the TD method shows an isolated minimum of the halocline base depth.

375 density ratio maximum which is related to a very steep temperature gradient (Fig. 5f) at the base of the PSW. While all three methods rely on finding a threshold, the search direction differs. Because the ST method searches upward, the warm PSW layer does not result in isolated depth minima (Figs. 5d and h). Overall, this analysis suggests that the search direction matters. With the DR and the TD method, we search downward, while with the ST method we search upward. This helps to explain why the ST method yields more robust results with fewer unexpected depth minima appearing in the basin-wise statistics discussed

380 below. For the DR method, on the other hand, Fig. 3a shows that the DR threshold is exceeded also far below the halocline base. Such local DR maxima below the halocline base were also found in the presence of thermohaline staircases (not shown here). Additional DR maxima below the halocline base, such as the one in Fig. 3, prevent us from simply reversing the search direction in the DR algorithm.

~~[M.A and I.P] Figure RM3 shows profiles of temperature, salinity, Turner angle, and stability sorted by the CHL base depth from~~

385 ~~the DR, the TD, and the ST method in a 3° radius around 74°N 145.5°W in the Beaufort Sea. Cases in which the criteria for detecting the CHL were not met were excluded. This resulted in a different number of profiles for each method. Included in Fig. RM3 are, however, cases in which the base depth of the CHL was set to the SML depth because the CHL base was diagnosed to either be above the SML base or coincided with the SML base to within 0.001 m, and which are otherwise also classified as "no CHL". The latter is rather often the case for the DR method, as evidenced by the numerous points in the~~

390 ~~upper left part of Fig. RM3b where the SML and CHL_{DR} base depth coincide. In between, there are many cases in which the CHL_{DR} base is located less than −30 m below the SML base, as evidenced be the numerous almost vertical lines in the upper~~
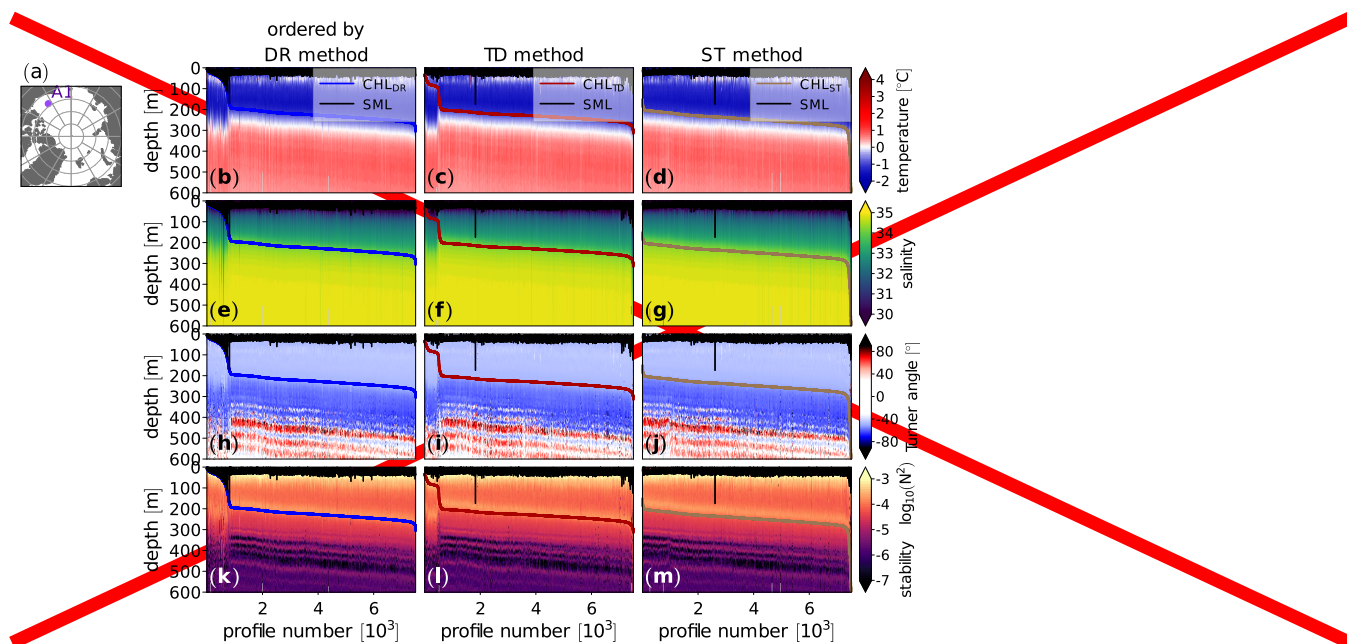
Figure RM3. **Please note: This figure was removed.** [M.A and I.P] ~~All used profiles of (b,c) temperature, (d,e) Turner angle and (f,g) stability profiles within 3° radius around 74°N 145.5°W (A1, shown in a) in the Beaufort Sea ordered by estimated cold halocline base depths (left CHL$_{DR}$, right CHL$_{ST}$). Lines are base depths of SML (black), cold halocline layer derived with DR method (blue), TD method (dark red) and ST method (brownish-gray).~~

~~right corner of Fig. RM3b. For the first few hundred profiles in Fig. RM3b, a cold and stable layer (CHL) that separates the mixed layer from the warmer water below is found underneath the line indicating the CHL base depth that was identified using the DR method (CHL$_{DR}$), indicating the occurrence of spurious CHL base depth minima.~~

395 [M.A and I.P] ~~The TD method also shows artifacts (Fig. RM3c). But compared to the DR method, it is somewhat less prone to locating the CHL base close to the SML in the presence of clear indications of a CHL in the temperature and salinity fields. In particular, there are nearly no cases in which the CHL$_{TD}$ base coincides with the SML base, and which would erroneously be classified as "no CHL". While none of the three methods is completely free of artifacts, the ST method (Fig. RM3d) appears to perform best under these particular conditions.~~

400 ### 3.2 Statistical comparison of the halocline base depth and occurrence frequency from different methods~~CHL occurrence frequency~~

[M.A and I.P] In order to identify differences between the methods used for halocline base detection regarding the geographical distribution of halocline base depth and halocline occurrence frequency (i.e. number of profiles for which a halocline base was detected divided by number of profiles analyzed) we used a simple nearest-neighbor (NN) averaging to produce maps (Fig. 6). 405 The underlying grid uses an azimuthal-equidistant projection with ∼0.47° resolution at the North Pole. [M.A.] In addition to these
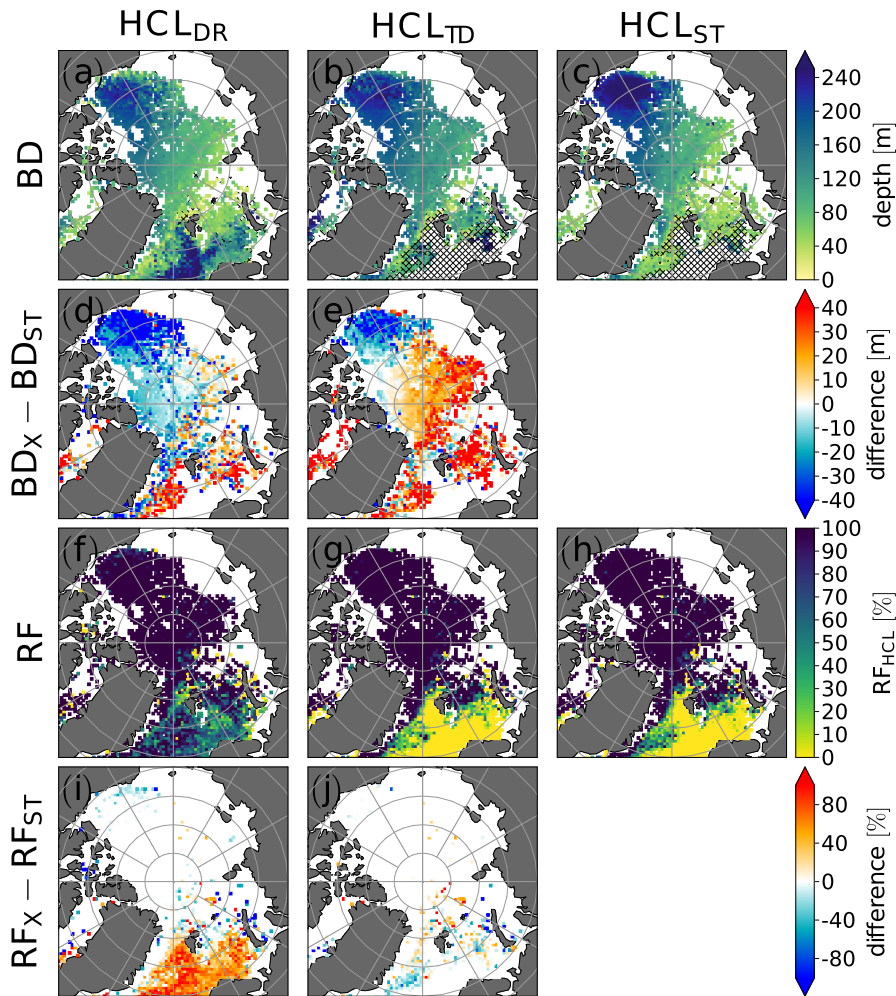
Figure 6. Please note: Revised and combined figure, based on figures 5 and 6 of the original manuscript. Kriging and SML maps are now excluded. We also excluded regions shallower than 100 m. The figure differs from the corresponding figure in our response to the reviewer comment by I. P. because we omitted low-resolution profiles form the UDASH data set as described in the revised manuscript. [M.A and I.P] Halocline base depth (BD) ~~Map of occurrence frequency of cold halocline~~ derived by [M.A and I.P] the (a,d) density-ratio [M.A and I.P] (DR) algorithm [M.A and I.P] **(a)**, [M.A and I.P] the (b,e) temperature-difference [M.A and I.P] (TD) algorithm [M.A and I.P] **(b)**, and [M.A and I.P] (c,f) the new stability [M.A and I.P] (ST) algorithm [M.A and I.P] **(c)**. Difference of HCL BD between the DR and the ST algorithm **(d)** and between the TD and the ST algorithm **(e)**. Relative frequency (RF) of HCL occurrence (i.e. number of profiles for which a halocline was detected divided by number of profiles analyzed) **(f–h)** and differences **(i–j)** as in (a–e). In (a–c), ~~Those were calculated by (a-c) simple nearest-neighbor averaging and (d-f) kriging~~ points where the relative occurrence frequency of the [I.P] HCL was ~~CHL is~~ below 1% were masked out. Hatching indicates regions where the [I.P] HC ~~CH~~ L occurrence frequency is below 25%. [I.P] Points where the ocean floor depth is below 100 m were masked out.

.

maps (which in data-rich regions show a time mean halocline base depth), we computed basin-wise statistics of halocline base depths. Figure 7 shows relative frequencies of halocline base depth diagnosed with the three methods for the Eurasian Basin, the Makarov Basin, and the Canada Basin.

[M.A and I.P]As expected, all three methods yield a similar overall spatial distribution of halocline base depth (Fig. 6a–c) with

410 shallower halocline base in the Eurasian Basin and the Makarov Basin compared to the Canada Basin. This spatial pattern is consistent with Polyakov et al. (2018). In the Eurasian Basin, the time averaged halocline base depth diagnosed with the DR method (Fig. 6a) and the ST method (Fig. 6c) agree relatively well, while the TD method overestimates halocline depth relative to both other methods (Fig. 6b). For the elliptical area covering the Eurasian Basin in Fig. 7a, the mean base depth was 85.9 m for the DR method and 92.3 m for the ST method vs. 116.1 m for the TD method. This overestimate of the halocline base depth

415 by the TD method compared to the other two methods is consistent with the previous result for ITP-74. Unlike the DR and the ST method, which both correctly identified the CHL base during the first months of ITP-74, the TD method placed the halocline base somewhere in the LHW. In addition to the moderate difference in the mean base depth between the DR and the ST method, the relative frequency of halocline base depth (Fig. 7b) in the Eurasian Basin reveals differences between the DR and the ST method, which are not reflected by the difference of the mean base depths. The ST method more often identifies a

420 shallow halocline base (< 60 m) in the Eurasian Basin compared to the DR method, which is consistent with the finding that the ST method apparently captures the start of new halocline formation from Sect. 3.1. More frequent detections of halocline bases not only above 60 m but also below 120 m with the ST method compared to the DR method account for a slightly wider halocline base depth distribution in the Eurasian Basin in the ST method compared to the DR method (Fig. 7b). The more frequent halocline base depths larger than 120 m in the ST method are likely related to an overestimate of halocline base depth

425 similar to the one found for the ST method for ITP-33 above. Slightly increasing the stability threshold in the ST method may lead to a better match between the halocline base depth estimate from the ST and the TD method by moving the halocline base estimated by the ST method upward and by decreasing the sensitivity of the ST method to new halocline formation. For the elliptical area covering the Makarov Basin in Fig. 7b, the DR method yielded a mean halocline base depth of 112.3 m, the ST method of 118.1 m, and the TD method of 133.5 m. For the elliptical area covering the Canada Basin, on the other hand, the

430 ST method yielded the largest mean halocline base depth. The mean halocline base depths for the Canada Basin corresponding to Fig. 7d are 191.4 m for the DR method, 206.6 m for the TD method, and 219.1 m for the ST method. In the Canada Basin (Fig. 7d), the ST method detected a halocline base shallower than 160 m for 0.05% of the profiles, while the DR method detected a halocline base shallower than 160 m for 10.2% of the profiles and the TD method for 3.5% of the profiles, indicative of isolated base depth minima due to the influence of warm PSW above PWW. Isolated minima very likely also contribute to

435 a more variable (noisier) halocline base depth in the Canada Basin in the map for the DR method in Fig. 6a and to a lesser extent also in the map for the TD method in Fig. 6b compared to the ST method (Fig. 6c). The larger average base depth in the Canada Basin in the ST method compared to both other methods (see also Fig. 6d and e) is, however, not only explained by the isolated depth minima in the DR and the TD method in Fig. 7d. Instead, more frequent depths greater than 260 m in the ST method compared to the other two methods (Fig. 7d) contribute to the greater average halocline base depth diagnosed with the

440 ST method, again indicating that a slight increase of the stability threshold in the ST method would lead to a better agreement

between the halocline base depth from the ST and the DR method. While a halocline was almost always detected in the Canada Basin by all three methods, the relative occurrence frequency (defined as the number of profiles in which a halocline base was detected divided by the total number of profiles which were analyzed) varies strongly in the Norwegian Sea (Fig. 6f–h). While the ST method and also the TD method very rarely detected a halocline base in the Norwegian Sea, the DR method frequently detected a halocline base in the Norwegian Sea. Furthermore, the DR method suggests a transition from a deeper halocline in relatively warm water inflow to a shallower halocline further north, which is absent in the other two methods (Fig. 6a–c). When using the DR method for analyzing halocline retreat in these warm water inflow regions, this may lead to different results compared to the two other methods. One reason for the DR method detecting a halocline base at depth could be thermohaline staircases. Overall, the largest differences in halocline detection frequency between the methods (Fig. 6i and j) were found in regions which are prone to sea ice retreat and, according to global climate model results, may also be particularly prone to events, in which large temperature gradients are found directly underneath the SML, and which mainly occur during winter (Metzner et al., 2020). [M.A and I.P] ~~The occurrence frequency of the CHL is analyzed in Fig. 6. Figure 6a to c shows occurrence frequencies based on simple nearest-neighbor (NN) averaging, and Fig. 6d to f time-averaged kriging results. As expected, all three methods detect a CHL in the Arctic Basin in most cases. However, even in the basin, the DR method yields numerous isolated minima in the nearest neighbor map (Fig. 6a). The occurrence frequency in the basins in the smoothed map from the DR method (Fig. 6d) is also lower compared to the other two methods.~~ [M.A and I.P] ~~Overall, the CHL occurrence frequency from the DR method shows evidence of noise. On the one hand, the observations from ITP 74 in Fig. **??** suggest a rather variable CHL base depth in the parts of the Central Arctic on the way towards the East Greenland Sea. On the other hand, Fig. RM3 and Supplement 1 suggest that some of the "no CHL" cases in which the CHL base was above the SML base are related to spurious minima in the CHL base depth.~~[M.A and I.P] ~~The potential role of spurious minima in the DR method can perhaps be best assessed by comparing the results from different methods. Because the ST and the TD method produce less artifacts while still capturing cases like the one in Fig. **??** for ITP 74, in which the SML deepened all the way to the Atlantic water, we deem the higher occurrence frequencies in the Arctic Basin based on the ST and the TD method more realistic compared to those based on the DR method.~~[M.A and I.P] ~~The situation outside the Central Arctic is more complicated, and not surprisingly, large differences between the three methods are found in the East Greenland Sea, the Barents Sea and the Atlantic. Two of the three methods occasionally detect a CHL in the Northern Atlantic, where only the TD method shows a near zero occurrence frequency (please refer to Supplement 2 for additional discussion of this issue).~~ In order to prevent the DR ~~and the ST~~ method from identifying a [I.P]halocline base~~CHL~~ in relatively warm water, one could either limit the region to which the method is applied (as Polyakov et al., 2018) or else introduce additional constraints on the water temperature. Limiting the region is clearly a sensible choice in a stable climate. However, limiting the region to a region in which a stable [I.P](cold) halocline~~CHL~~ is found at most times limits us in studying regional shifts. With regard to shifts due to climate change, one should be aware that methods differ regarding requirements for halocline base identification and results~~how cold the CHL must be~~.

3.3 [M.A and I.P]~~Maps of CHL boundaries~~
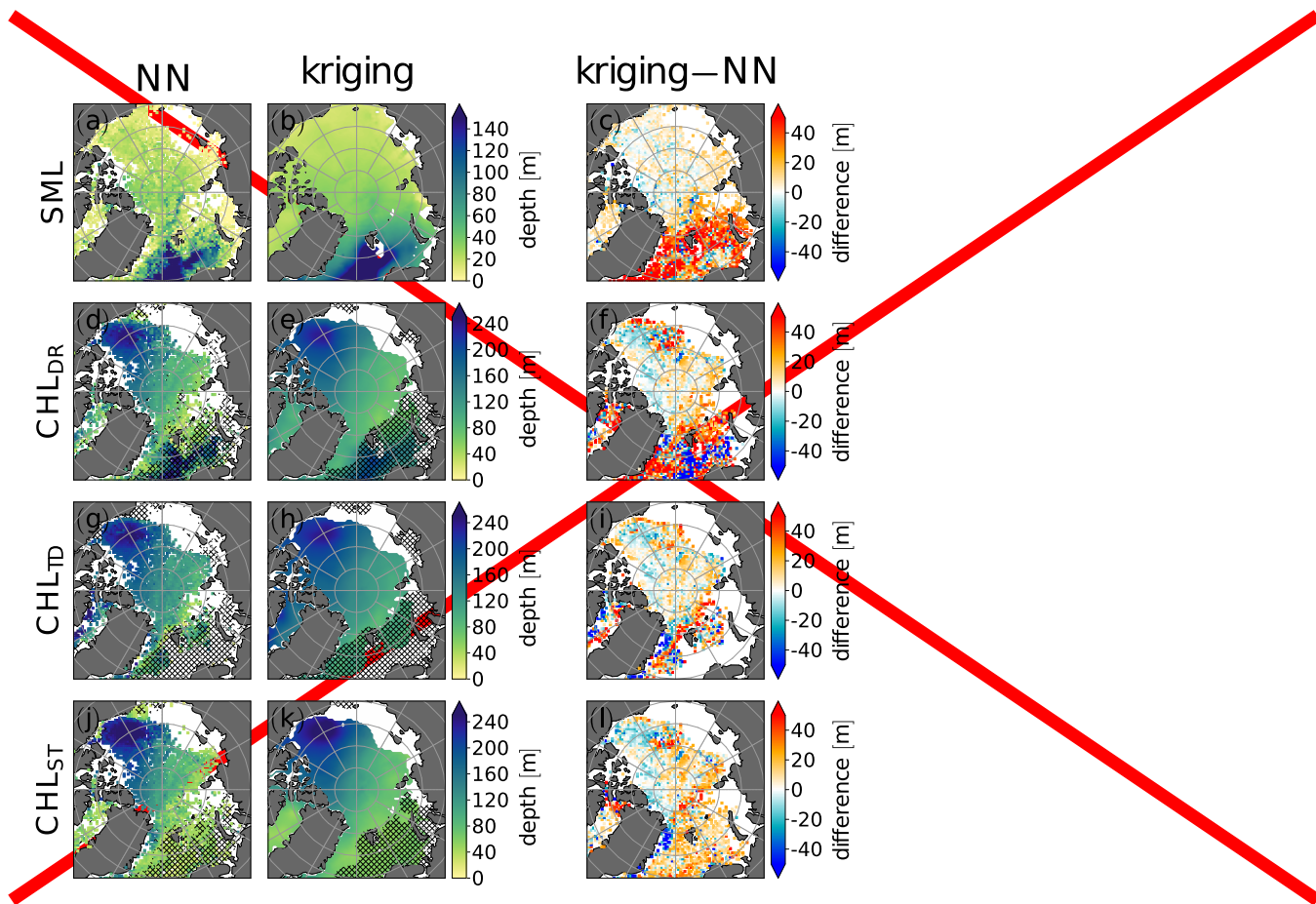
Figure RM5. **Please note: This figure was revised and combined with the preceding figure.**[M.A and I.P] ~~Comparison of (left) simple nearest-neighbor averaging to (center) kriging results with (right) difference plot for (a–c) thickness of SML and CHL base depth derived by (d–f) DR method, (g–i) TD method and (j–l) the new ST method. Points where the relative occurrence frequency of the CHL is below 1% were masked out in (d–c). Hatching indicates regions where the CHL occurrence frequency is below 25%. The SML depth in the East Siberian Sea and the interior of the Laptev Sea is based on observations in summer and fall.~~

[M.A and I.P] ~~Figure RM5a shows the mean base depth of the SML (top of the CHL) as identified by a change in potential density of~~
475 ~~0.125 kg m^{-3} based on NN-averaging. The map that results from kriging and the difference between the two maps are shown in Figures RM5b and c. The annual mean SML depth in the East Siberian Sea and the interior of the Laptev Sea in Fig. RM5a and b is most likely underestimated because of a lack of data in winter and spring.~~

[M.A and I.P] ~~The SML depth gradient with a comparatively deep annual mean SML in the Barents Sea, intermediate values in the Eurasian basin, and a comparatively shallow annual mean SML in the Amerasian Basin and the Chukchi Sea in Fig. RM5a~~
480 ~~and b is in line with Fig. 14 of Peralta-Ferriz and Woodgate (2015).~~

^{M.A and I.P}Although kriging acts to smooth the field, Fig. RM5b still shows some small scale variability in the Central Arctic, which may result from relatively sparse observations in winter and spring (Fig. ??) in combination with a fairly pronounced seasonal cycle (Fig. RM6).

^{M.A and I.P}The time mean CHL base depths determined from the DR method (Fig. RM5d, e), the TD method (Fig. RM5g, h), and the ST method (Fig. RM5j, k) show a similar overall pattern. Comparatively deep time mean CHL bases below 200 m are found in the Canada Basin. The CHL base depth decreases as one moves from the Canada Basin through the central Amerasian Basin and then across the North Pole into the Eurasian Basin. This overall pattern is consistent with figures 4g and h of Polyakov et al. (2018). This CHL base depth gradient is roughly opposite to the gradient of the SML depth.

^{M.A and I.P}There are, however, several notable differences between the methods to determine the CHL base depth. For example, the TD method yields somewhat larger CHL base depths over the Central Arctic compared to the DR and the ST method. A particularly striking difference in Fig. RM5 is found for the CHL base depth in the Barents Sea. While CHL occurrence frequencies in the Barents Sea are fairly low for all three methods, they differ notably, depending on which method is used to detect the CHL base (Fig. 6). For the DR method, the CHL base depth decreases from the Barents Sea toward the Central Arctic. This contrasts the finding by Steele et al. (1995) that the CHL forms in the Barents Sea and deepens where Atlantic water sinks at the slopes north of the Barents Sea into the Eurasian Basin. On the other hand, complex situations similar to the one observed by ITP 74 are difficult to capture by methods that to some extent rely on simplification. We nevertheless chose to include the Atlantic and the Barents Sea in our comparison, in part because it helps to highlight problems, which with increasing atlantification may also occur in other regions.

^{M.A and I.P}Furthermore, as indicated above, the CHL occurrence frequency in the Barents Sea is generally low. Especially for the TD method, a CHL is rarely detected in the Barents Sea (Fig. 6b). Because the CHL base depth is only computed for cases in which a CHL is detected, the time mean SML depth in Fig. RM5 often exceeds the time mean depths of the CHL in the Atlantic and also the Barents Sea.

^{M.A and I.P}The kriged CHL base maps (Figures RM5e, h, k) are smoother compared to the kriged SML map (Fig. RM5b), in part because of a smaller seasonal cycle (Fig. RM6). Artifacts in the DR method are partially filtered out here because spurious depth minima in the CHL base often reach the SML, so that these cases are not taken into account in computing the mean CHL base depths.

3.4 ^{M.A and I.P}SML and CHL base depth seasonality

^{M.A and I.P}The seasonality of the SML and the CHL base depths are investigated in Fig. RM6. Insufficient data availability is an issue especially in the East Siberian Sea and the interior of the Laptev Sea, where both the seasonal cycle of the SML depth and the CHL base depth are most likely underestimated because of the absence of observations in winter and spring. The SML base depth varies more strongly with season than the CHL base depths for the East Greenland Sea, the Barents Sea, and the Atlantic. Together with the different spatial gradients in annual mean depths, this presumably makes the CHL in these regions more prone to ventilation events in winter, such as the ones investigated by Polyakov et al. (2018). This stronger seasonal cycle
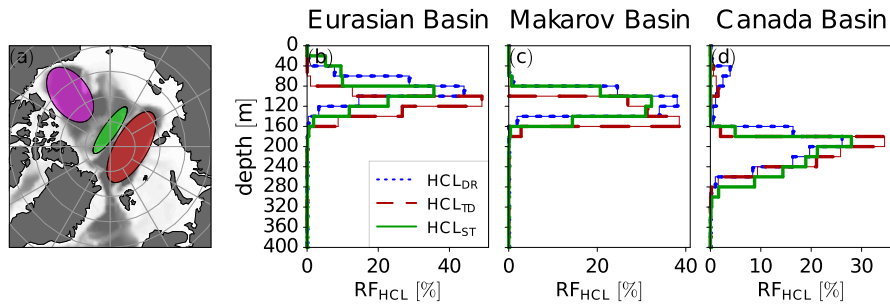
Figure 7. **Please note: Figure added based on suggestion by M.A. This plots differ from the corresponding plots in our response to the reviewer comment by M. A. mainly because the version of the plots in the discussion was accidentally based on a dataset which was meant for kriging, and from which outliers had been removed as described in the original version of the manuscript, and also because we omitted low resolution profiles form the UDASH data set as described in the revised manuscript.**[M.A.] Map showing elliptical areas over the Canada Basin (purple), the Makarov Basin (green) and the Eurasian Basin (dark red) and ocean floor depth (grey shading) **(a)**. Relative frequency of halocline (HCL) base depth determined with the density ratio (DR), temperature difference (DR) and the stability (ST) method for the elliptical areas over the Eurasian Basin **(b)**, the Makarov Basin **(c)**, and the Canada Basin **(d)**.

515 ~~of the SML is also generally consistent with our finding from models that CHL thinning events were most frequent in winter and spring, when the SML is deep (Metzner et al., 2020).~~

[M.A and I.P]~~In the Amerasian Basin and the Chukchi Sea, the seasonal cycle of the SML depth is much smaller, often with maximum depths in March and April (Fig. RM6u). The CHL base depth on the other hand, shows a seasonal cycle also near the Chukchi Shelf in the Canada Basin (e.g. Fig. RM6h,l,p, and t), which could be an effect of Pacific water entering through the Bering Strait. In parts of the East Siberian Sea, the maximum SML thickness is reached in autumn (Fig. RM6u), but this is~~

520 ~~probably an artifact due to insufficient data availability.~~

[M.A and I.P]~~Differences between methods in CHL base depth for the individual seasons occur mainly in regions in which also the CHL occurrence/detection frequency varied. This again warrants a note of caution when applying these methods in the regions which are most prone to changes in the CHL occurrence frequency. Outside these regions, the seasonal cycle of the CHL base depth is largely consistent across the methods.~~

525 [M.A and I.P]~~For example, in winter, the CHL base depths increases almost across the entire Arctic. Only the TD method shows moderate decreases in the East Greenland Sea and north of the Barents Sea. A reason for the decrease might be that the TD method is more prone to not detecting any CHL at all in winter either because the SML base is below the CHL base that would otherwise have been detected or else because the condition on the water temperature is not met. For the cases in which a CHL is detected, it is shallower. Furthermore, because of the kriging, regions with near-zero CHL occurrence frequency can be more~~

530 ~~strongly affected by neighboring regions.~~
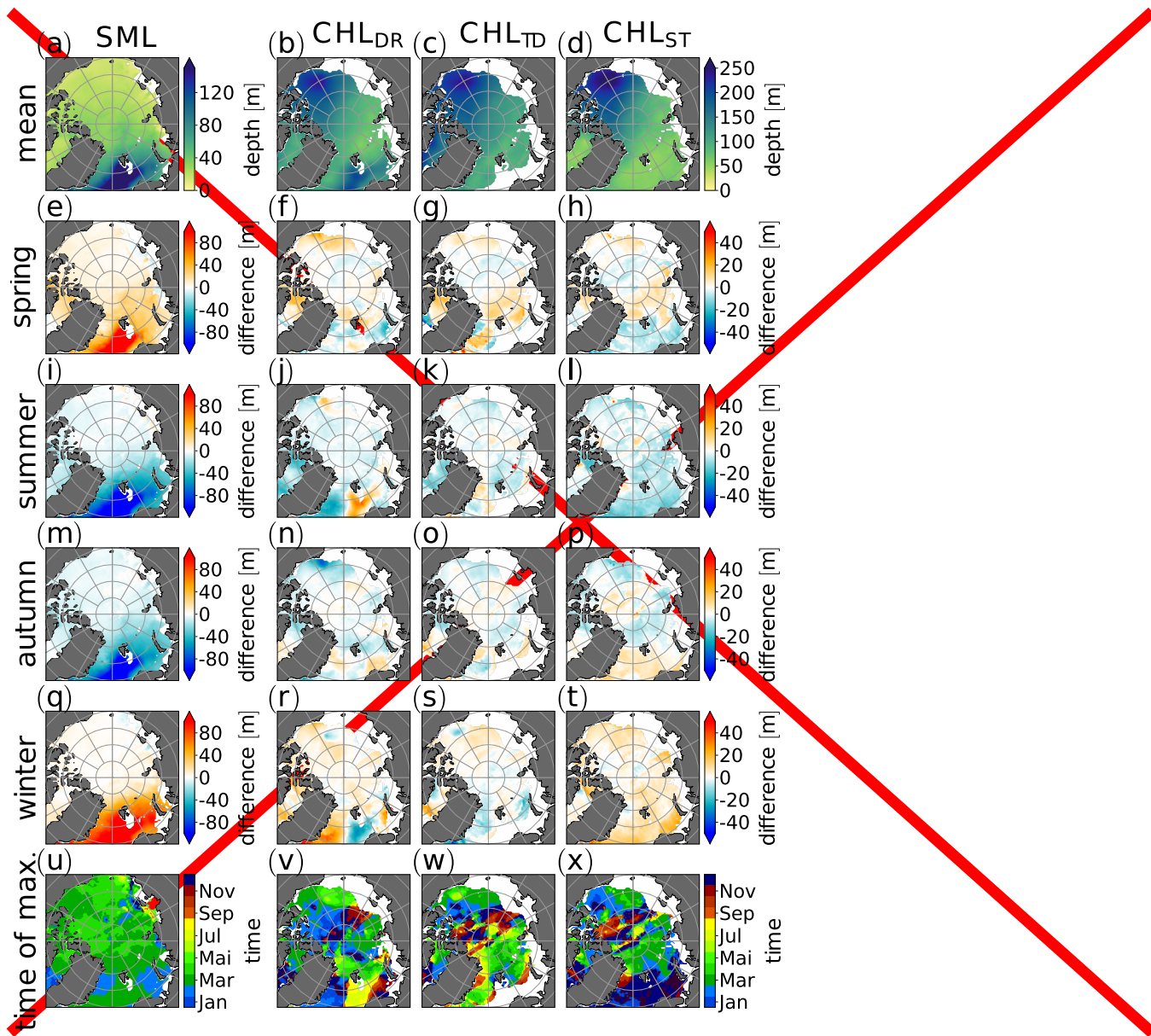
Figure RM6. ~~Please note: This figure was deleted.~~ [M.A and I.P] ~~Annual mean of (a) SML depth, CHL base depth derived by (b) the density-ratio method, (c) the temperature-difference method, and (d) the new stability method. The corresponding seasonal means are shown in (e) to (f). The phase of the seasonal cycle in (u) to (x) is estimated via a cosine fit.~~

3.5 Estimation of cold halostad boundaries

In the Canada Basin, the PWW forms a so-called cold halostad, while the LHW is modified water of Atlantic origin. This leads to a local vertical stability minimum between two local vertical stability maxima (Fig. 5d and h). The upper vertical stability maximum is associated with an increase of salinity near the top of the PWW and the lower stability maximum is associated

535 with an increase in salinity between PWW and LHW. The local minimum of vertical stability between these two local maxima is associated with a small salinity gradient around the core of the PWW (Fig. 5a and e)~~the CHL structure is more complex and features an upper layer and a lower layer (Shimada et al., 2005). This is for example reflected by the bimodal vertical stability profile in Fig. ?? along the track of ITP 33~~. The new algorithm described in Sect. 2.2 was designed to provide estimates for the location of the cold halostad layer [I.P]boundaries and the center, where the center is assumed to be the mean depth between

540 the upper and the lower boundary. T~~which lies between these two halocline layers. The~~ top and base depth timeseries derived with the new algorithm are shown by dark green lines in ~~(~~Fig. 4~~)~~. T~~At the moment t~~he algorithm wa~~si~~s designed to avoid misclassifications of the cold halostad by requiring the difference between~~vertical extent of~~ the lower stability~~'~~ maximum ~~valley'~~ and the stability minimum (i.e. the depth of the 'stability valley') to be ~~(a)~~ at least 0.2. Furthermore, the vertical extent of the 'stability valley' was required~~orders of the squared Brunt-Väisälä-frequency and (b)~~ to be greater than 50 m. This leads

545 ~~(a)~~ to occasional discontinuities~~breaks~~ in the cold halostad boundary. ~~lines~~ Fig. 4 shows such discontinuities as evidenced by the breaks in the dark green lines. Furthermore, the requirement of a minimum depth leads to~~visible for ITP 29 in Fig. ?? and (b)~~ shallow halostad layers not being detected.

Collecting all available observations with detected cold halostad bound~~eri~~es per grid cell leads to the map[I.P]s of [I.P]CHS center depth and CHS thickness~~the cold halostad~~ shown in Fig. 8[I.P]a and b. The main occurrence region of the cold halostad is

550 the Canada Basin, where Pacific water circulates between the SML and water of Atlantic origin~~Atlantic water~~ (Shimada et al., 2005). Employing conservative assumptions to avoid a misclassification (including a lower bound of 50 m for the thickness), we detect a cold halostad layer in the Canada Basin region in Fig. 8b ∼70–90% of the time, except in August, September, and October when the occurrence frequency is slightly below 70% (Fig. 8c). In August, September, and October the fraction of grid points for which observations were available within the Canada Basin region was also particularly high (red line

555 in Fig. 8c). Based on Fig. 1~~Therefore~~, more points at the edge of the Canada Basin ~~region in~~ region in Fig. 8b, where the occurrence frequencies decrease, may have been included in the analysis during these month. Furthermore, a cold halostad was detected near the coasts of Greenland where glacial cold water acts similar to the Pacific [M.A and I.P]low salinity~~semi-saline~~ water (Dmitrenko et al., 2017).

4 Summary and discussion

560 We introduced a new method for determining the [I.P]halocline~~CHL~~ base depth based on vertical stability and~~,~~ compared it to [M.A.]the density ratio and the temperature difference method. Our main motivation for using a vertical stability threshold instead of a DR or TD threshold was that vertical stability is more closely related to the role of the halocline as a stable layer which separates the SML from warmer AW below and thus acts to protect sea ice. Another objective was to design a particularly
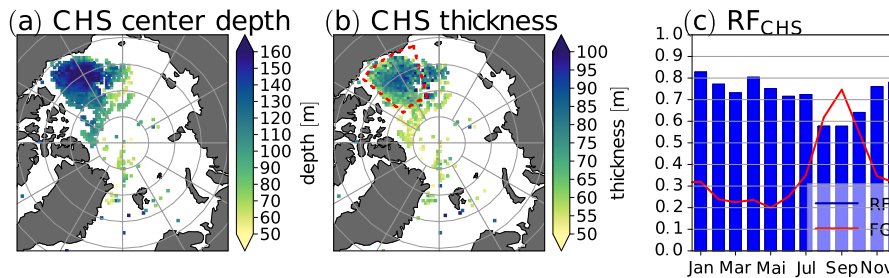
Figure 8. Map of mean **(a)** [I.P]CHS center depth and **(b)** [I.P]CHS thickness[I.P] ~~of derived cold halostad~~. **(c)** Monthly relative occurrence frequency ~~fraction~~ (RF$_{CHS}$, blue bars) of the CHS~~cold halostad~~ in the Canada Basin region (area enclosed by red dashed lines in (b) and fraction of grid points (FG) for which at least one observation was available in the respective month (red line).

robust method. We also devised a new stability-based method to identify the CHS, which is formed by PWW in the Canada
565 Basin and also by melt water off the eastern coast of Greenland and Svalbard.~~two existing methods, and combined two existing comprehensive observational datasets to study the upper layers of the Arctic Ocean, generating maps of SML depth, CHL base depth, and also cold halocline depth and thickness for cases in which the cold halostad is thicker than 50 m and an additional requirement for the vertical extent of the stability minimum is fulfilled.~~ To our knowledge, this is the first time that ~~such~~ a method for detecting the CHS has been devised and tested~~applied to a comprehensive dataset~~.

570 [M.A and I.P]We found that the DR and the new ST method both correctly identified the base of the CHL in the Eurasian Basin during the first months of ITP-74, while the TD method placed the halocline base somewhere in the LHW. Furthermore, the analysis of individual profiles after convection in ITP-74 indicated that the new ST method captured the beginning of new halocline formation via the convective homogenization and subsequent fresh water capping mechanism proposed by Rudels et al. (1996). In the Canada Basin, the new method overestimated the halocline base depth compared to the DR method, which
575 correctly identified the halocline base for ITP-33. This disagreement between the DR and the ST method could be reduced by slightly increasing the stability threshold in the ST method. Slightly increasing the stability threshold (which is at present based on an approximate relationship between density ratio and stability) may lead to a better agreement of halocline base depth between the DR and the ST method not only by moving the halocline base from the ST method upward but also by decreasing the sensitivity of the ST method to new halocline formation.

580 Unlike the two existing methods, the new ST method to detect the halocline~~CHL~~ base yielded few artificial halocline~~CHL~~ base depth minima. [I.P]In the two existing methods, such artifacts were found to be associated with warm PSW on top of cold PWW in the Canada Basin. Because the new method searches for the halocline base from below, such artifacts were avoided, leading to a more robust method, especially compared to the widely used DR method. Unfortunately, because of DR maxima below the cold halocline base (which are for example associated with thermohaline staircases), the search direction in the DR
585 method cannot simply be reversed in order to increase the robustness also of the DR method.

A particularly striking difference between the DR~~new~~ method and the other two ~~existing~~ methods was found in the [I,P]Norwegian ~~Barents~~ Sea. [I,P]While the ST and the TD method almost never detected a halocline in the Norwegian Sea, the DR method frequently detected a halocline base in the Norwegian Sea. Remarkably, the halocline in the DR method decreased north of the Norwegian Sea. This intriguing difference between the methods should be taken into account, for example when studying the effects of warm AW inflow on the cold halocline, especially because warm water inflow regions are particularly prone to react to anthropogenic warming (although the effects of warming on either accelerating or preventing new halocline formation are manifold and changing over time, and destabilization of an existing stable halocline by warming form below is only one potential contributor to increased annual mean net surface heat fluxes from the ocean to the atmosphere in warm water inflow regions found in climate models)~~For the DR method, the CHL base depth decreased from the Barents Sea toward the Central Arctic. This contrasts the finding by Steele et al. (1995) that the CHL forms in the Barents Sea and deepens where Atlantic water sinks at the slopes north of the Barents Sea into the Eurasian Basin~~.

[M.A and I.P]~~The lack of a requirement for water temperature in the DR and the new ST method was found to be problematic as one approaches the Atlantic and may be problematic when applying these methods in a warmer climate. Although an additional constraint on the water temperature could be applied in combination with the DR and the ST method in order to decrease the number of false CHL detections in comparatively warm water, it would come at the cost of decreasing the sensitivity to the vertical salinity gradient. The problem of detecting a CHL base in comparatively warm water is altogether avoided by the TD method, which is highly sensitive to warming from below, but not directly (or only implicitly) to changes in salinity.~~

[M.A and I.P]~~Because differences between the methods to detect the CHL bottom exist, one should always strive to ensure that the outcome from such methods is consistent with the raw data and beware of limitations in different regions. Unfortunately, our study suggests that the results from different methods to determine the CHL base depth tended to differ most in those regions in which the CHL was expected to be most affected by current climate change. Better understanding the properties of different methods can help to choose between more and less appropriate methods, based on the specific scientific question.~~

[M.A and I.P]Regarding the new method for CHS detection, a case study and an application to a comprehensive dataset yielded encouraging results. The case study suggested that the method correctly identified a layer with a small vertical salinity gradient formed by PWW. This small salinity gradient led to a stability minimum between two local stability maxima which was captured by the new stability method for CHS detection. ~~We also suggested a method that attempts to identify the cold halostad based on stability. To our knowledge, this is the first time that such a method has been devised and applied to a comprehensive dataset.~~ Because we found it necessary to introduce a constraint~~s~~ on the cold halostad thickness and to set a threshold requirement for the magnitude~~the depth~~ of the stability minimum, our method suffers from a low detection sensitivity and altogether misses cold halostad layers that are thinner than 50 m. Nevertheless, a cold halostad was frequently detected in the Canad~~ian~~ B~~b~~asin throughout the year and the number of missed detections tended to be small as for ITP-33, while some other ITPs yielded almost perfect results and some other ITPs slightly worse results (not shown). This suggests that a stability-based method for CHS detection could be useful for future studies exploring variability and changes of the CHS in the Canada Basin.

620   One method to advance cold halostad and [I,P]halocline base~~CHL~~ detection in the future may lie in the application of artificial intelligence. This would require a-priori manual classification applied to a training and an evaluation dataset. In the absence of objective criteria that work under most circumstances, such manual classification would ultimately have to rely on expert judgment, which may in turn introduce a different set of problems. Given the various shortcomings of traditional threshold methods, AI-based methods could nevertheless be useful.

625 *Code and data availability.* The Ice tethered profiler data (Krishfield et al., 2008; Toole et al., 2011) used in this paper are taken from the website of the Ice-Tethered Profiler program based on Woods Hole Oceanic institution via https://www2.whoi.edu/site/itp/ (last access 23 January 2022). The UDASH-dataset (Behrendt et al., 2018) is available from the PANGAEA data archive at http://doi.org/10.1594/PANGAEA.872931. [M.A and I.P]~~The Java code for the kriging software developed by E.P.M is available at https://github.com/spatzewind/JKriging/releases/tag/v0.0.5 in version 0.0.5 (doi:10.5281/zenodo.7572759).~~

630 *Author contributions.* E.P.M. devised the new method for determining the Arctic Ocean cold halocline and cold halostad layer depths and performed the data analysis. Both authors contributed equally to writing the manuscript.

Competing interests. The authors declare that they have no conflict of interest.

Acknowledgements. We thank the two reviewers, I. Polyakov and M. Athanase, for their very insightful and very constructive comments, especially for their suggestions regarding the analysis of individual profiles, new halocline formation, the structure of the introduction, and
635 basin-wise statistics, which we consider a major contribution to our revised manuscript. The Ice-Tethered Profiler data were collected and made available by the Ice-Tethered Profiler Program based at the Woods Hole Oceanographic Institution (http://www2.whoi.edu/site/itp). We gratefully acknowledge the funding by the Deutsche Forschungsgemeinschaft (DFG, German Research Foundation) - Projektnummer 268020496 - TRR 172, within the Transregional Collaborative Research Center "ArctiC Amplification: Climate Relevant Atmospheric and SurfaCe Processes, and Feedback Mechanisms (AC)^3". We thank J. Chylik for comments that helped to improve the readability of our
640 manuscript.

References

Aagaard, K., Coachman, L. K., and Carmack, E.: On the halocline of the Arctic Ocean, Deep Sea Res. Part I Oceanogr. Res. Pap., 28, 529–545, https://doi.org/10.1016/0198-0149(81)90115-1, 1981.

Alkire, M. B., Polyakov, I., Rember, R., Pnyushkov, A., Ivanov, V., and Ashik, I.: Combining physical and geochemical methods to investigate lower halocline water formation and modification along the Siberian continental slope, Ocean Sci., 13, 983–995, https://doi.org/10.5194/os-13-983-2017, 2017.

Anderson, L. G., Andersson, P. S., Björk, G., Jones, E. P., Jutterström, S., and Wåhlström, I.: [I.P]Source and formation of the upper halocline of the Arctic Ocean, J. Geophys. Res. Oceans, 118, 410–421, https://doi.org/10.1029/2012jc008291, 2013.

Athanase, M.: Review on the manuscript EGUSPHERE-2023-106, EGUsphere, https://doi.org/10.5194/egusphere-2023-106-RC2, 2023.

Baumann, T. M., Polyakov, I. V., Pnyushkov, A. V., Rember, R., Ivanov, V. V., Alkire, M. B., Goszczko, I., and Carmack, E. C.: On the seasonal cycles observed at the continental slope of the eastern Eurasian Basin of the Arctic Ocean, J. Phys. Oceanogr., 48, 1451–1470, https://doi.org/10.1175/JPO-D-17-0163.1, 2018.

Behrendt, A., Sumata, H., Rabe, B., and Schauer, U.: UDASH – Unified Database for Arctic and Subarctic Hydrography, Earth Syst. Sci. Data, 10, 1119–1138, https://doi.org/10.5194/essd-10-1119-2018, 2018.

Bertosio, C., Provost, C., Sennéchael, N., Artana, C., Athanase, M., Boles, E., Lellouche, J.-M., and Garric, G.: The western Eurasian Basin halocline in 2017: Insights from autonomous NO measurements and the Mercator Physical System, J. Geophys. Res. Oceans, 125, e2020JC016 204, https://doi.org/10.1029/2020JC016204, 2020.

Bertosio, C., Provost, C., Athanase, M., Sennéchael, N., Garric, G., Lellouche, J.-M., Kim, J.-H., Cho, K.-H., and Park, T.: Changes in Arctic halocline waters along the East Siberian Slope and in the Makarov Basin from 2007 to 2020, J. Geophys. Res. Oceans, 127, https://doi.org/10.1029/2021jc018082, 2022.

Björk, G., Söderkvist, J., Winsor, P., Nikolopoulos, A., and Steele, M.: Return of the cold halocline layer to the Amundsen Basin of the Arctic Ocean: Implication for the sea ice mass balance, Geophys. Res. Lett., 29, 1–8, https://doi.org/10.1029/2001GL014157, 2002.

Bourgain, P. and Gascard, J. C.: The Arctic Ocean halocline and its interannual variability from 1997 to 2008, Deep Sea Res. Part I Oceanogr. Res. Pap., 58, 745–756, https://doi.org/10.1016/j.dsr.2011.05.001, 2011.

Deng, G. and Cahill, L.: [M.A.]An adaptive Gaussian filter for noise reduction and edge detection, in: 1993 IEEE Conference Record Nuclear Science Symposium and Medical Imaging Conference, vol. 3, pp. 1615–1619, IEEE, San Francisco, CA, USA, https://doi.org/10.1109/nssmic.1993.373563, 1993.

Deutsch, C. V.: [M.A and I.P]Kriging with strings of data, Math. Geol., 26, 623–638, https://doi.org/10.1007/BF02089245, 1994.

Dmitrenko, I. A., Kirillov, S. A., Rudels, B., Babb, D. G., Pedersen, L. T., Rysgaard, S., Kristoffersen, Y., and Barber, D. G.: Arctic Ocean outflow and glacier–ocean interactions modify water over the Wandel Sea shelf (northeastern Greenland), Ocean Sci., 13, 1045–1060, https://doi.org/10.5194/os-13-1045-2017, 2017.

GEBCO Bathymetric Compilation Group 2021: The GEBCO_2021 grid - a continuous terrain model of the global oceans and land., https://doi.org/10.5285/c6612cbe-50b3-0cff-e053-6c86abc09f8f, 2021.

Gill, A. E.: Atmosphere-ocean dynamics (International Geophysics Series, Volume 30), Academic Press, 1982.

Janout, M. A., Hölemann, J., Timokhov, L., Gutjahr, O., and Heinemann, G.: Circulation in the northwest Laptev Sea in the eastern Arctic Ocean: Crossroads between Siberian River water, Atlantic water and polynya-formed dense water, J. Geophys. Res. Oceans, 122, 6630–6647, https://doi.org/https://doi.org/10.1002/2017JC013159, 2017.

Jensen, M. F., Nilsson, J., and Nisancioglu, K. H.: The interaction between sea ice and salinity-dominated ocean circulation: implications for halocline stability and rapid changes of sea ice cover, Clim. Dyn., 47, 3301–3317, https://doi.org/10.1007/s00382-016-3027-5, 2016.

680 Jones, E. P. and Anderson, L. G.: [I,P]On the origin of the chemical properties of the Arctic Ocean halocline, J. Geophys. Res., 91, 10 759, https://doi.org/10.1029/jc091ic09p10759, 1986.

Kikuchi, T., Hatakeyama, K., and Morison, J. H.: [I,P]Distribution of convective Lower Halocline Water in the eastern Arctic Ocean, J. Geophys. Res., 109, https://doi.org/10.1029/2003jc002223, 2004.

Krishfield, R., Toole, J., Proshutinsky, A., and Timmermans, M.-L.: Automated ice-tethered profilers for seawater observations under pack
685 ice in all seasons, J. Atmos. Ocean Technol., 25, 2091–2105, https://doi.org/10.1175/2008JTECHO587.1, 2008.

Lien, V. S. and Trofimov, A. G.: Formation of Barents Sea branch water in the north-eastern Barents Sea, Polar Res., 32, https://doi.org/10.3402/polar.v32i0.18905, 2013.

Lin, P., Pickart, R. S., Våge, K., and Li, J.: Fate of Warm Pacific water in the Arctic Basin, Geophys. Res. Lett., 48, e2021GL094 693, https://doi.org/10.1029/2021GL094693, e2021GL094693 2021GL094693, 2021.

690 Lind, S., Ingvaldsen, R. B., and Furevik, T.: Arctic layer salinity controls heat loss from deep Atlantic layer in seasonally ice-covered areas of the Barents Sea, Geophys. Res. Lett., 43, 5233–5242, https://doi.org/10.1002/2016GL068421, 2016.

Macdonald, R. W., Kuzyk, Z. A., and Johannessen, S. C.: [I,P]It is not just about the ice: a geochemical perspective on the changing Arctic Ocean, J. Environ. Stud. Sci., 5, 288–301, https://doi.org/10.1007/s13412-015-0302-4, 2015.

Mert, B. A. and Dag, A.: A computer program for practical semivariogram modelling and ordinary kriging: A case study of porosity
695 distribution in an oil field, Open Geosci., 9, 663–674, https://doi.org/10.1515/geo-2017-0050, 2017.

Metzner, E. P., Salzmann, M., and Gerdes, R.: Arctic Ocean surface energy flux and the cold halocline in future climate projections, J. Geophys. Res. Oceans, 125, e2019JC015 554, https://doi.org/10.1029/2019JC015554, 2020.

Mu, L., Zhao, J., and Zhong, W.: Regime shift of the dominant factor for halocline depth in the Canada Basin during 1990–2008, Acta Oceanol. Sin., 36, 35–43, https://doi.org/10.1007/s13131-016-0883-0, 2017.

700 Peralta-Ferriz, C. and Woodgate, R. A.: Seasonal and interannual variability of pan-Arctic surface mixed layer properties from 1979 to 2012 from hydrographic data, and the dominance of stratification for multiyear mixed layer depth shoaling, Prog. Oceanogr., 134, 19–53, https://doi.org/10.1016/j.pocean.2014.12.005, 2015.

Polyakov, I.: Review of the manuscript (egusphere-2023-106) entitled "Technical note: Determining Arctic Ocean cold halocline and cold halostad layer depths based on vertical stability" by E. P. Metzner and M. Salzmann, EGUsphere, https://doi.org/10.5194/egusphere-2023-
705 106-RC1, 2023.

Polyakov, I. V., Pnyushkov, A. V., Alkire, M. B., Ashik, I. M., Baumann, T. M., Carmack, E. C., Goszczko, I., Guthrie, J., Ivanov, V. V., Kanzow, T., Krishfield, R., Kwok, R., Sundfjord, A., Morison, J., Rember, R., and Yulin, A.: Greater role for Atlantic inflows on sea-ice loss in the Eurasian Basin of the Arctic Ocean, Science, 356, https://doi.org/10.1126/science.aai8204, 2017.

Polyakov, I. V., Pnyushkov, A. V., and Carmack, E. C.: Stability of the Arctic halocline: a new indicator of Arctic climate change, Environ.
710 Res. Lett., 13, https://doi.org/10.1088/1748-9326/aaec1e, 2018.

Polyakov, I. V., Rippeth, T. P., Fer, I., Alkire, M. B., Baumann, T. M., Carmack, E. C., Ingvaldsen, R., Ivanov, V. V., Janout, M., Lind, S., Padman, L., Pnyushkov, A. V., and Rember, R.: Weakening of cold halocline layer exposes sea ice to oceanic heat in the eastern Arctic Ocean, J. Clim., 33, 8107–8123, https://doi.org/10.1175/JCLI-D-19-0976.1, 2020.

Reshid, T. M.: Kriging and simulation in Gaussian random fields applied to soil property interpolation, Am. J. Theor. Appl. Stat., 8, 296–305,
715 https://doi.org/10.11648/j.ajtas.20190806.21, 2019.

Roquet, F., Ferreira, D., Caneill, R., Schlesinger, D., and Madec, G.: Unique thermal expansion properties of water key to the formation of sea ice on Earth, Sci. Adv., 8, https://doi.org/10.1126/sciadv.abq0793, 2022.

Rudels, B., Anderson, L. G., and Jones, E. P.: Formation and evolution of the surface mixed layer and halocline of the Arctic Ocean, J. Geophys. Res. Oceans, 101, 8807–8821, https://doi.org/10.1029/96JC00143, 1996.

720   Rudels, B., Jones, E. P., Schauer, U., and Eriksson, P.: [1,P]Atlantic sources of the Arctic Ocean surface and halocline waters, Polar Res., 23, 181–208, https://doi.org/10.3402/polar.v23i2.6278, 2004.

Shimada, K., Itoh, M., Nishino, S., McLoaughlin, F., Carmack, E., and Proshutinsky, A.: Halocline structure in the Canada Basin of the Arctic Ocean, Geophys. Res. Lett., 32, https://doi.org/10.1029/2004GL021358, 2005.

Steele, M. and Boyd, T.: Retreat of the cold halocline layer in the Arctic Ocean, J. Geophys. Res., 103, 10 419–10 435,
725   https://doi.org/10.1029/98JC00580, 1998.

Steele, M., Morison, J., and Curtin, T.: Halocline water formation in the Barents Sea, J. Geophys. Res., 100, 881–894, 1995.

Timmermans, M.-L., Proshutinsky, A., Golubeva, E., Jackson, J. M., Krishfield, R., McCall, M., Platov, G., Toole, J., Williams, W., Kikuchi, T., and Nishino, S.: Mechanisms of Pacific Summer Water variability in the Arctic's Central Canada Basin, J. Geophys. Res. Oceans, 119, 7523–7548, https://doi.org/10.1002/2014jc010273, 2014.

730   Toole, J. M., Krishfield, R. A., Timmermans, M.-L., and Proshutinsky, A.: The ice-tethered profiler: ARGO of the Arctic, Oceanography, 24, 126–135, http://www.jstor.org/stable/24861307, 2011.

Zhong, W., Steele, M., Zhang, J., and Cole, S. T.: Circulation of Pacific Winter Water in the Western Arctic Ocean, J. of Geophys. Res. Oceans, 124, 863–881, https://doi.org/10.1029/2018jc014604, 2019.